DOE/ER/40224-214

DOE/ER/40224--214

DE92 014320

PROGRESS REPORT

DISCLAIMER

1. INTRODUCTION

The experimental high energy physics group at the University of Oregon has focussed its effort during the last year on its ongoing experimental program at the Stanford Linear Collider (SLC) and on the plans for the experiments at the Superconducting Super Collider (SSC). At the SLD, the group has been active in the commissioning of the SLD experiment, with the engineering run being completed in August, 1991. Three members of the group (Cary Zeitlin, Kevin Pitts, and Hwanbae Park), have been in residence at SLAC and still are. Cary Zeitlin has been responsible for the commissioning of the SLD small angle calorimetry system, which includes the SLD luminosity monitor that was built at Oregon during the past year. For the SSC, the group has joined the GEM Collaboration and has been very active in the preparation of the plans and documentation for this proposed experiment.

The Oregon GEM effort concentrates on the calorimeter and pre-radiator; Jim Brau presently serves as co-organizer of the calorimeter group for GEM. The Oregon contribution to the GEM emergence has been substantial.

In concert with the GEM Detector preparation, the Oregon group is working on the silicon electromagnetic calorimeter subsystem under the SSC R&D program.

The Oregon group is also a part of the U.S. Tau-charm Collaboration and has been working on detector design issues for this proposal. If approved, this experiment would be built and collect data after SLD and before the SSC begins running. It fits naturally into the physics plans of the group and promises to lead to very important physics measurements.

David Strom joined the Oregon group as an assistant professor in September, 1991. He comes from the Opal Collaboration, and is exploring participation in the Opal upgrade of the luminosity monitor to a silicon sandwich calorimeter, similar in some respects to the SLD luminosity monitor built by the Oregon group. He has become active in GEM since coming to Oregon.

The progress of the Oregon group on all of these effort has been quite significant during the past year, as will be documented in the sections to follow.

2. SLD

2a. 1991 Engineering Run

The SLD Engineering Run of 1991 succeeded in delivering the first Z^0 events to SLD. 379 events have been found in the off-line analysis. The physics readiness of the SLD detector was demonstrated by the measurement of physics such as the 2, 3, and 4-jet fractions. More importantly, the SLC achieved all its major performance goals. Table I demonstrates this.

Table I. SLC Achievements
(Mark II was the 1990 detector.)

	Typical 1990	Typical 1991	Goal 1991	Achieved 1991
$e^-(10^{10})$	3.3	3.0	4.0	4.7
$e^+(10^{10})$	1.9	3.0	3.0	3.8
e^+ Yield	0.6	1.0	1.0	1.25
$e^- x - emittance(10^{-5}m)$	8	3	5	
$e^- y - emittance(10^{-5}m)$	3.5	2.5	3	
$e^+ x - emittance(10^{-5}m)$	3.5	2.7	3	
$e^+ y - emittance(10^{-5}m)$	3.5	2.7	3	
$e^-@IP(10^{10})$	2.5	2.8	3.5	
$e^+@IP(10^{10})$	1.5	3.0	2.5	
$< \sigma > (\mu m)$	3.3	2.2	2.2	
Rep Rate (Hz)	120	60	120	
Reliability		60%	30%	
Z/hr	4@120 Hz	5@60 Hz	15@120 Hz	8@60 Hz
Total Z's			300-500	370 on tape

2b. LMSAT-25 Construction, Installation, and Commissioning

The SLD luminosity monitor construction was completed at the University of Oregon during 1991. By mid-1990, the silicon wafers had all been received and tested at the University of Oregon. The silicon was tested for both capacitance and leakage current at three different voltages. They were also visually inspected and measured for proper alignment. Since Hamamatsu Photonics supplied test results with each detector, the Oregon tests were to verify the Hamamatsu results and insure that no damage was incurred during shipping.

The machine shop at the University of Oregon fabricated the 90% tungsten radiator and support structure for the LMSAT. The LMSAT-25 uses 96 radiator plates. Each plate is 3.5 mm thick with 12 drilled and tapped holes with tight tolerances for proper alignment of the silicon wafers. In addition, assembly and installation tooling were fabricated in the University of Oregon machine shop.

The design improvements of the LMSAT-25 led to the use of 50 conductor cables to carry the signals from 20 cells. The connections on the electronics packages require 34 conductor connectors carrying 16 signals. A custom board was designed to route four sets of 20 signals into five sets of 16 signals. Since space was constrained, the signal router boards were designed to lie outside the detector yet inside of the available space.

The four silicon-tungsten modules which comprise the SLD LMSAT-25 (Luminosity Monitor/Small Angle Tagger) were assembled at the University of Oregon in early March. After assembly, the modules were flown to SLAC where they were again tested to verify that they were not damaged during transit.

The SLD Engineering Run took place in the Spring and Summer of 1991. The MASC was installed in SLD in January of 1991, just prior to SLD's move onto the SLC beamline. The LMSAT-25 was installed on the SLD beamline in late April and early May. Previously, an earlier version of the LMSAT (LMSAT-16) was installed on the North end of the SLD beamline, primarily for the purpose of developing an installation procedure. No serious attempt was made to read the system out at that time. This time, however, the start of the engineering run was imminent, so a full-scale installation was in order. The principal tasks were:

- Install both North and South LMSAT-25 modules.
- Connect cables from LMSAT and MASC to electronics. This was a major chore, due to extremely dense packaging and inflexible cables (we are examining options for more flexible cables).
- Install both electronics packages, and verify that they work.

- Install the sheet metal fins and cooling loop used to regulate the electronics temperature. The cooling loop was connected to the water supply for the first time; leaks in the loop and/or connections cannot be tolerated.

- String cables in the South (the North had been cabled during the earlier practice installation).

- Install temperature sensors, special diodes with implanted α sources, and dosimeters to measure the integrated dose received by the detector and electronics.

Some additional constraints were imposed for the real installation: the closing of the SLD doors requires strict observation of very tight radial stay-clears for our equipment, cables, etc.; the system was to be inaccessible for a period of 3 months; and there was considerable pressure to finish quickly, since the LMSAT was the last system installed prior to door-closing. Given the time pressure and the low priority of temperature and α source monitoring, we chose to concentrate our efforts on making sure the calorimeter could be read out reliably.

In the period immediately following LMSAT installation and SLD door-closing, several rounds of tests were conducted to guarantee that the SLD's self-shielding was adequate. One of the tests of shielding involved dumping the high-intensity SLC beams on a beam-stop just upstream of the detector, thus flooding the SLD with muons. It was immediately obvious that, at the very least, the LMSAT was sensitive, as it showed a high occupancy of low-energy hits with the beam in this condition. Individual muons were identified in a few events, showing roughly the expected pulse heights.

By late June, the SLD had been certified as providing adequate shielding, and attempts began to collide the e^+ and e^- beams with tolerable backgrounds. The first trickle of Bhabha events in the LMSAT and Z° events in the rest of SLD came in early July. By the time the run ended in mid-August, the SLD had collected some 340 Z° events and over 1400 Bhabha events in a well-defined fiducial volume. (Most of the data were collected in the last two weeks of the run, when SLC's efforts were concentrated on improving SLD's integrated luminosity and machine physics studies were given low priority. For most of the run, priority was given to machine physics.)

We consider the SLD Engineering Run to have been a very successful period of commissioning for the LMSAT. Major milestones included:

- Successful operation of the calorimeter and electronics over a period of three months with no access.

- Development of on- and off-line code to identify Bhabhas and reject background.
- Understanding threshold factors that allow the SLD to trigger on Bhabha events without significant deadtime, in spite of considerable backgrounds.
- Identification of a "golden" fiducial region in which the Bhabha detection efficiency is virtually 100% and the background is negligible, even with loose cuts on the data.
- Identification of a second region with 75% Bhabha detection efficiency (tighter cuts are needed to eliminate background), which can be used to cross-check results from the golden region.

The performance of the calorimeter was quite good. Figure 1 shows a typical Bhabha event seen in the LMSAT-25.

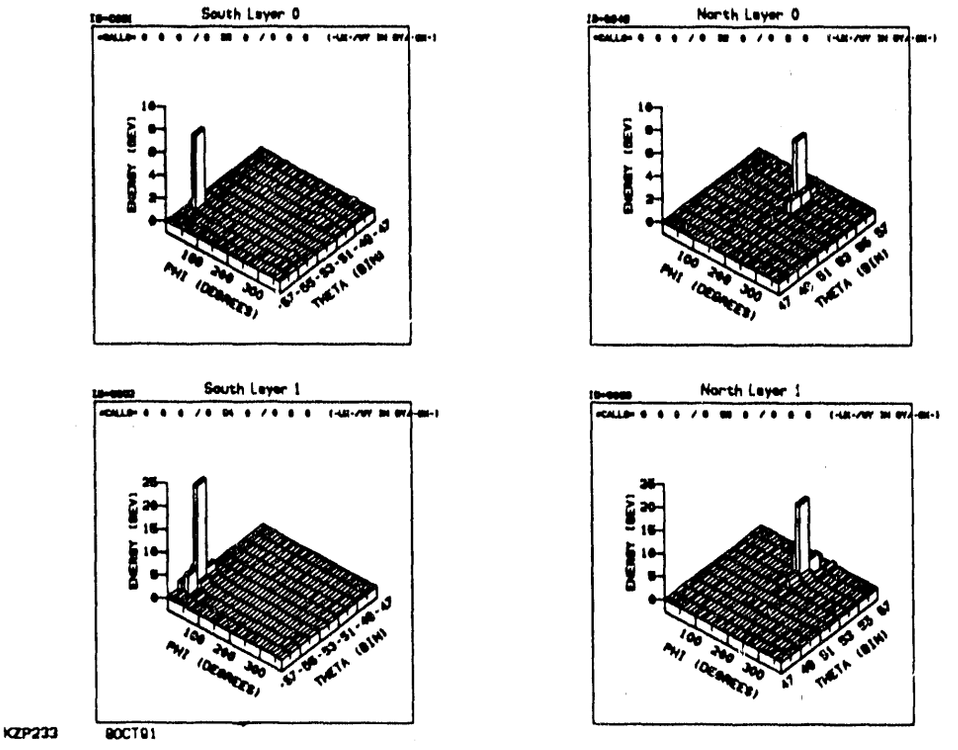

Figure 1. Bhabha scattering event

The energy resolution obtained agrees very well with Monte Carlo calculations as is shown in figure 2. The position resolution is excellent as well: 500 microradians in θ, and 10 milliradians in ϕ. Work is continuing to see if the position resolution can be improved; an extrapolation from our test-beam data leads us to believe that factors of $\sim$ 1.5 may be obtainable. Understanding the position resolution (and hence the inner acceptance boundary) is essential to minimize the systematic error associated with the luminosity measurement.

A copy of our IEEE NSS paper describing this subsystem is attached as an appendix.

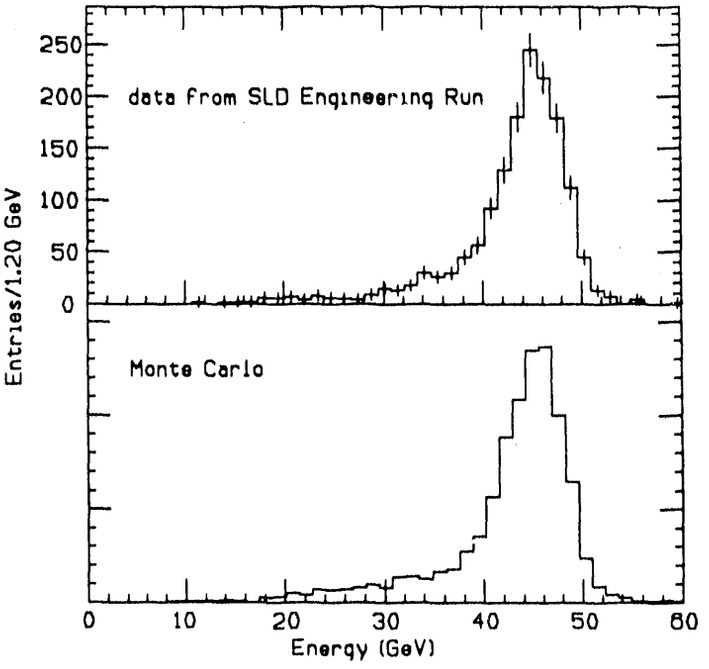

Figure 2. Energy seen in the LMSAT–25 for Bhabha events

2c. SLC Software Work

Cary Zeitlin devoted a fraction of his time during the past year on the final focus of the SLC. Specifically, Cary has written software to control the position of the superconducting final focus (SCFF). The following is some background information.

The size of the beam is related to the emittance by $\epsilon = \theta\sigma$ where θ is the angular divergence of the beam. For purposes of the final focus, the emittance can be considered a constant produced by the machine. (Much of the anticipated program of SLC improvements centers on reducing the emittance throughout the machine.) Naively, one might simply hope to focus the beams to as small a spot as

possible, without regard to the angular divergence. However, experience with the Mark II detector shows a strong correlation between increasing angular divergence and background seen in the detector. The background comes from synchrotron photons which scatter into the detector and convert into low-energy pairs.

Successful operation of the SLC/SLD thus depends critically on the performance of the SCFF. Given good magnet behavior, the most important factor affecting the SCFF is its alignment. Several members of the SLD, including Cary Zeitlin of the Oregon group, have entered into an ongoing dialogue with SLC experts to solve the hardware and software issues surrounding SCFF alignment. While the SLC is running, it is most convenient for personnel in the Main Control Center (MCC), and using the MCC Vax, to have the ability to move the SCFF in order to study the effects on spot size and backgrounds. (The diagnostic tools already exist, and make use of beam-beam deflection signals seen in downstream monitors.) However, the SCFF is part of SLD and must be moved when the doors open and close; therefore the hardware and software which control SCFF motion must reside on the SLD Vax. Cary Zeitlin has written the software which takes an operator-requested movement of the SCFF and turns it into the appropriate commands to the stepper motor controllers.

3. MARK II

The Mark II detector took its last data in Fall 1990 at the SLC. Analysis of the data has continued over the last year. This analysis has been primarily focused on the data of the last running period, which included the precision vertex detectors: a silicon-strip detector inside of a precision wire vertex detector. These detectors performed very well. Unfortunately, the data sample during this period was only a few hundred Z^0 decays. However, the precision of these devices allowed for physics results, including publications, conference presentations, and PhD dissertations. (See Ray Frey's C.V. for the references.)

Analysis of other aspects of the data have also continued, involving PEP data, SLC data, or a combination. Ray Frey and Jingchen Zhou of the Oregon group have become involved in an analysis of multi-particle dynamics of hadronic final states, often referred to as "intermittency" studies. These studies search for non-Poissonian fluctuations in the multiplicity density of charged particles in rapidity and/or azimuth, and provide new tools by which to compare particle production with the underlying physics. It is hoped that firstly these studies can provide more sensitive tests of monte carlo descriptions of fragmentation and hadronization, for example like that of the LUND monte carlo program. Secondly, a better understanding of of the connection between particle production and non-perturbative QCD might result. (For references, see recent conference proceedings. For example the Proc. of the Sante Fe Workshop on Intermittency in High Energy Collisions, March 1990; or the Proc. of the XXVth International Conference on High Energy Physics, Singapore, August 1991.)

William Murray and Harold Ogren of Indiana University have been studying intermittency in Mark II data, and in Summer 1991, the Oregon group began working with them. A paper, to be submitted to Physical Review, is in preparation which will utilize the fact that the Mark II detector took data both at $\sqrt{s}$ =29 and 91 GeV to directly compare the energy dependence of the phenomena.

4. GEM

The Oregon group has work for several years on the design and study of general purpose high p_T detectors for the SSC. This year the SSCL was unable to approve either of the competing detectors, L^* or EMPACT/Texas, and called on the community to consider developing an alternative second detector. In June of 1991, a new collaboration, the GEM Collaboration, was formed. By July 8, 1991, the collaboration had prepared an expression of interest which was submitted to the SSCL. This produced a positive reaction from the SSC Program Advisory Committee, and at this time a letter of intent is in preparation for submission on November 30, 1991. During the intervening five months the GEM Collaboration has developed a detector concept which promises to complement the other general purpose high p_T detector, SDC.

The principal physics justification of the SSC is the elucidation of the electroweak symmetry breaking. This is the central physics focus of the GEM Detector. The search for the Higgs boson or bosons therefore plays center stage, as well as searches for other competing symmetry breaking mechanisms: technicolor or supersymmetry, for example. Additionally, searches for new quarks, leptons, Z's, W's, substructure, or other unexpected new phenomena are planned.

With these physics goals in mind, the design of the GEM detector has led to the following characteristics to maintain complementarity to SDC:

1. Precision muon momentum measurement in an open geometry outside the calorimeter;
2. High precision electromagnetic calorimetry, without the handicap of an inner magnetic coil;
3. Hermetic, projective hadronic calorimetry with adequate energy resolution ($\sim 50\%/\sqrt{E}$);
4. Central tracking in the magnetic field.

These detector concepts produce an experiment optimized to attack the physics goals stated above. The detector is being designed to ensure operation at the highest possible luminosities ($\gtrsim 10^{34} cm^{-2} sec^{-1}$).

4a. GEM Calorimetry

The calorimeter is a crucial element of the proposed detector. Jim Brau of the Oregon group was appointed co-organizer of the calorimeter subgroup in July, 1991, shortly after the formation of the GEM Collaboration. Initially, the calorimeter

group evaluated the numerous concepts that were proposed by collaborators, to define a few viable and desirable options. The calorimeter group has held the goal of precision electromagnetic calorimetry high, and has arrived at two approaches to this goal.

The electromagnetic calorimetry is crucial for searching for the Higgs boson in the mass range 80-130 MeV/c^2. Excellent electromagnetic calorimetry is achievable either with crystal calorimetry with excellent stability, or with fine sampling calorimetry. The GEM Collaboration is purusing both of these avenues until one clearly establishes itself as the best approach.

The crystal calorimetry approach is based on BaF_2 crystals. Interest in barium fluoride arose years ago[1] when it was discovered to be an inherently radiation hard medium. Subsequent experience has revealed that the radiation environment of the SSC may exceed its tolerance. The two outstanding issues to be demonstrated for barium fluoride are its cost and its radiation hardness. The cost issue is addressed through agreement with Chinese manufacturing. The radiation hardness requires improved understanding of the damage mechanisms. Presently, the best preliminary understanding[2] of the damage mechanism is:

- Radiation damage is associated with some particular cationic impurities, including Pb and Ce. Many other metallic impurities which are important in BGO, such as Fe, do not have a harmful effect in BaF_2.
- When oxygen is absorbed in the crystals, during the pretreatment or growing process, $O^{2-}F^{+}$ dipoles are formed.
- When the crystal is irradiated, the $O^{2-}F^{+}$ dipoles decompose. This leads to increased absorption in the 190-250 nm region from O^{2-} ions and in the visible from F-centers formed by the fluorine.
- The damage is reversible by exposing the crystal to UV light, which frees the fluorine from the F-centers and results in reassociation of the $O^{2-}F^{+}$.

With this understanding of the fundamental damage mechanism, development of radiation hard crystal fabrication is concentrating on higher purity raw materials for crystal growth and more tightly controlled pretreatment of the raw materials to control oxygen contaminants.

Research and development on the liquid argon option emphasizes extending the successful evolution of accordion calorimetry. Accordion geometry calorimeters, which have been constructed[3] at CERN using 2 mm thick absorber plates, have been able to achieve electromagnetic resolutions of better than $10\%/\sqrt{E}$. This

resolution must be improved to meet the GEM goal of $7.5\%/\sqrt{E} \oplus 0.5\%$. The GEM calorimeter group will pursue this improved performance in more than one way. First, an accordion calorimeter based on 1 mm plates will be built and tested. Secondly, a 2 mm geometry will be tested with liquid krypton as the sampling medium. Finally there is a tentative plan to develop a plate calorimeter with strip-line readout.

4b. Silicon Preradiator

Physics goals of the SSC and the role of a preradiator

The program of the Silicon Electromagnetic Calorimeter Collaboration (SECC), supported by SSC subsystem R&D funding, was expanded during the past year to include the development of a silicon preradiator. The initial plan adopted the devices and procedures of the electromagnetic calorimeter to a modular 3, 4, or 5 layer silicon preradiator.

The potential of lepton and single-γ identification as physics tags motivates the deployment of a preradiator at the SSC. Numerous physics goals benefit from this subsystem: heavy Higgs, intermediate mass Higgs, top searches and studies, direct photon production, as well as more exotic studies such as Z' and heavy quarks. The excellent electron identification and π^0 rejection of the preradiator could contribute significantly to these physics studies.

For an example of the deployment of a silicon preradiator, consider the GEM calorimeter with a silicon strip preradiator. The pixel structure of a silicon strip preradiator offers important advantages over other techniques in the electron/hadron rejection which can be achieved. The overlap of complicated events, for example, is much simplified with a pixel detector. A "pixel" here would have a rectangular shape with dimensions of approximately 1 mm $\times$ 64 mm.

A silicon preradiator deployed in front of the GEM calorimeter would enhance considerably the capability for identification and measurement of electrons and photons. Such a preradiator could determine the centroid of an electromagnetic shower with a precision of better than 0.5 mm in both transverse coordinates. Additionally, the signature for two overlapping electromagnetic showers (the signature of a π^0) would be observable in many cases. The main advantages of a preradiator would be:

- Reduction of the $\pi^{\pm}$ contamination in the electron sample by at least a factor of 10 over bare calorimeter cuts by discriminating against charged tracks which deposit very little energy in the preradiator.

- Suppression of electron sample contamination by the accidental overlap of charged tracks with γ's by detecting a small displacement between the charged track trajectory and the origin of the shower.
- Enhancement of the tagging of b-quark jets by electrons by resolving electron showers even when they are comparatively close to the jet axis.
- Measurement of the direction of γs by combining the preradiator measurement of the initiation point of γ- induced showers with the shower centroid from the calorimeter.
- Discrimination of single γ's from π^0's by observing the origination of both showers in the π^0 case.
- Tagging of the beam crossing bucket for an electromagnetic shower; for slower calorimeter technologies this may be useful.

Several technologies are being proposed for preradiator subsystems. The advantages that a silicon strip preradiator offers are:

Pad/strip structure- no ghosts or shadowing

Projective in 2D

Spatial resolution < 0.5 mm

Two track resolution ~ 3.0 mm

Fast (single bunch response)

Only 15k readout channels

The unfavorable attributes are:

Specialized readout (limited to 3-4 bits/channel) to be developed

Multiplexing required for 15k readout channels

Two track resolution ~ 3.0 mm (limits π^0 veto)

A preradiator detector samples an electromagnetic cascade while introducing a minimal interaction probability, to use the well-defined development of electromagnetic cascades to eliminate hadrons. A preshower detector that emphasizes both longitudinal and transverse shower definition is clearly more powerful than one which chooses only longitudinal. By similar reasoning one which uses two-dimensional transverse shower size information is more powerful than one which operates in projection. The two-dimensional shape information allows one to detect e/γ overlaps as well as the unpleasant cases in which a pion undergoes a

charge-exchange reaction in the first converter plate, giving a lovely electromagnetic cascade, but with a p_T kick away from the incident direction. The GEM Collaboration must strive to devise a robust electron detector over the entire energy range of interest (50 GeV - 5 TeV) with sufficiently redundant electron identification power on "normal" events so that the rare events of interest in the SSC can be tagged unambiguously.

This argues for a silicon strip preshower detector. The two- dimensional information will be a powerful additional handle for electron tagging within high-p_T jets, compared with projective devices. The collection speed and rate capabilities of silicon are very important in the SSC environment. Moreover, the charged particle flux in the SSC produces negligible radiation damage. Only the albedo neutron flux must be tolerated, and the silicon detectors may be less sensitive than the tracking devices and readout, depending on choices for the detector.

To reiterate, the strengths of silicon are:

- ease of segmentation into arbitrary pixel geometry
- fast silicon signal collection to minimize event pileup
- pixel geometry to minimize pileup within one interaction
- absolute gain calibration, uniform throughout the detector
- minimal support and readout needs

In the early stages of shower buildup the transverse spread of the electromagnetic cascade about the incoming particle direction is limited to a small fraction of the Moliere radius that describes the mature cascade. This tight energy cluster is an important signature of an electron, and it also serves to aid in isolating electron candidates within a jet. Projective devices, for example, have more trouble with hadron/photon pileup within a jet. A two-dimensional measurement will give maximum rejection power.

The electronics for the silicon preshower detector can be simpler than for the full calorimeter. The dynamic range is lower and the capacitance is smaller. The charge is lower, so the ADC can be simpler, faster, and lower power than for the calorimeter in general, with fewer bits. There will be enough channels in the device to warrant dedicated electronics. The cost should be cheaper for silicon than for other detector candidates, since less signal processing is required on the preamp outputs to achieve the speed required.

Simulation of the preradiator

Although the preradiator will serve a very important role in electron identification, its function in rejection of π^0 backgrounds is crucial and very challenging. For example, π^0 background rejection demanded by the search for the Higgs boson in its decay to two photons requires stellar performance. We choose this process as a benchmark to assess the performance of the preradiator in rejection.

Figure 1 presents a few important distributions in the $H \rightarrow \gamma\gamma$ process for a 100 GeV Higgs. These plots show the gamma energies, the gamma pseudorapidities, the gamma transverse momenta, and the correlation of gamma energy with pseudorapidity. We note that a cutoff in pseudorapidity at 2.5 truncates the high end of the energy distribution.

Figure 2 shows the optimal rejection power of a preradiator that requires separation of the two gammas by 2, 3, or 6 mm in x or y as a function of the π^0 momentum divided by the pathlength from the π^0 decay to the preradiator. Also shown is the histogram for the γ's produced in the 100 GeV Higgs decay to $\gamma\gamma$ to illustrate the region of required coverage. One sees the need for a system which is able to reject at the 3 mm level.

Figure 3 is a repeat of the plots shown in figure 1, after a set of standard cuts have been applied. Here the gammas are required to have pseudorapidities in the range -2.5 to 2.5, to have transverse energies in excess of 20 GeV, and to have angles in the gamma-gamma rest frame such that $|cos\theta^*_\gamma| < 0.8$.

In figure 4 (on the left) we have for each of the gammas of figure 3, computed the optimal rejection (assuming the 3 mm capability above) taking into account the true path-length to the preradiator in the GEM Detector configuration. (We assume a nominal GEM configuration with a radius of 750 mm and a barrel length of 3000 mm.) We see a large fraction of these γ's are in the region of energy and pseudorapidity where the probability for rejection of background π^0's is at its highest. The right hand part of this figure presents the correlation of optimal rejection power with pseudorapidity. Here we note good performance in the barrel while the endcap region shows significance degradation.

Figures 5 and 6 present the pulseheight profiles for 50 GeV π^0s decaying with the minimal opening angle. These figures assume a one meter pathlength from decay to the preradiator. This corresponds to the GEM configuration at about $\eta = 1.0$. The bin size is 0.2 mm. Figure 5 shows the first four such events generated to give some feeling for the event-to-event fluctuation and figure 6 shows the distribution for a sum of 500 events. So far magnetic field effects have been neglected in these studies.

Another important issue which we have investigated in the context of the EMPACT/Texas Detector is that of electromagnetic energy resolution and the degra-

dation of such when the preradiator is placed in front of the electromagnetic calorimeter. In principle, a measurement of the energy deposited in the preradiator can be used to correct the calorimeter energy measurement and restore the resolution of the calorimeter. In a study of the EMPACT/Texas Liquid Argon Calorimeter with an energy resolution of $7.5\%/\sqrt{E}$ it was found that it was only necessary to measure the pulseheight in a layer behind the three radiation length preradiator to achieve full correction. This result was reported in "The Effect of a Pre-radiator on the Electromagnetic Energy Resolution for the EMPACT/TEXAS Liquid Argon Calorimeter," EMPACT/TEXAS Note #341, November 19, 1990.

4c. Physics Studies for GEM LoI

The Oregon group has been involved in simulations to understand the issues of hadronic jet reconstruction resolution for GEM. This is essentially GEM's answer to the PAC's query regarding mass resolution for reconstructing the hadronic final states for

1. $Z^0 \rightarrow q\bar{q}$
2. $Z' \rightarrow q\bar{q}$, where $M(Z') = 1$ TeV/c^2

Hong Ma of BNL has been primarily responsible for the former, and Ray Frey for the latter. Because time has been too short to develop a GEANT detector description and analysis, simple parametrizations of resolution effects have been used. In the case of Z', events were generated using sensible coupling constants in the Pythia monte carlo. Final, decayed particle 4-vectors were fed to calorimeter cells. The energy resolution for individual particles was included with the form $\sigma_E/E = \sqrt{a^2/E + b^2}$. Lateral shower spreading for hadrons was simulated with a simple analytical form. The calorimeter cells were then subjected to a jet-finding algorithm, and the mass of the jet-jet pair formed. An example of a resulting jet-jet mass distribution is shown in Fig. 7. In this case the resolution parameters were $a(em) = 0.075$, $b(em) = 0.005$, $a(had) = 0.50$, and $b(had) = 0.02$. The resolution for $Z^0 \rightarrow q\bar{q}$ is quite important for the process $H \rightarrow ZZ \rightarrow q\bar{q}l^+l^-$, where $l = e, \mu$. Performing a tight cut on the jet-jet mass near M_Z is a potentially powerful tool for enhancing the Higgs signal.

Koichiro Furuno has been simulating the process $H \rightarrow ZZ^*$. In the difficult "intermediate mass" region for the Higgs particle, that is for 100 GeV/c$^2 \lesssim M_H \lesssim 2M_Z$, GEM has focused on two discovery processes. One is the $H \rightarrow \gamma\gamma$ mode, and the other is the $H \rightarrow ZZ^*$ decay. The latter mode is especially important for a Higgs mass which is not too far below the threshold for real Z^0 pair production, where the signal/background for the $\gamma\gamma$ decay becomes poor.

References

1. S. Majewski and D. Anderson, Nucl. Instr. Meth. **A241**, 76 (1985).
2. H. Newman, private communication.
3. "Performance of a Liquid Argon Electromagnetic Calorimeter with an 'Accordian' Geometry", B. Aubert, *et al.*, CERN-PPE-91-73, April 1991.

FIGURE CAPTIONS

1) Distributions in the $H \rightarrow \gamma\gamma$ process for a 100 GeV Higgs. These plots show the gamma energies, the gamma pseudorapidities, the gamma transverse momenta, and the correlation of gamma energy with pseudorapidity. We note that a cutoff in pseudorapidity at 2.5 truncates the high end of the energy distribution.

2) The optimal rejection power of a preradiator that requires separation of the two photons by 2, 3, or 6 mm in x or y as a function of the π^0 momentum divided by the pathlength from the π^0 decay to the preradiator. Also shown is the histogram for the γ's produced in the 100 GeV Higgs decay to $\gamma\gamma$ to illustrate the region of required coverage.

3) Repeat of figure 1 after a set of standard cuts have been applied. Here the gammas are required to have pseudorapidities in the range -2.5 to 2.5, to have transverse energies in excess of 20 GeV, and to have angles in the $\gamma - \gamma$ rest frame such that $|cos\theta^*_\gamma| < 0.8$.

4) Left: we have for each of the gammas of figure 3, computed the optimal rejection (assuming the 3 mm capability above) taking into account the true path-length to the preradiator in the GEM Detector configuration. We see a large fraction of these γ's are in the region of energy and pseudorapidity where the probability for rejection of background π^0's is at its highest. Right: The correlation of optimal rejection power with pseudorapidity. Here we note good performance in the barrel while the endcap region shows significant degradation.

5) The pulseheight profiles for 50 GeV π^0s decaying with the minimal opening angle. The bin size is 0.2 mm. The first four such events generated are shown.

6) Same as Fig. 5 but for 500 events.

7) Two-jet mass distribution for simulated Z' hadronic decays in GEM. The Z' mass is 1 TeV/c^2. The points are the the monte carlo events, and the curve

is a fit of a gauscian on a polynomial. The indicated σ and M are the fitted rms and mean of the gaussian.

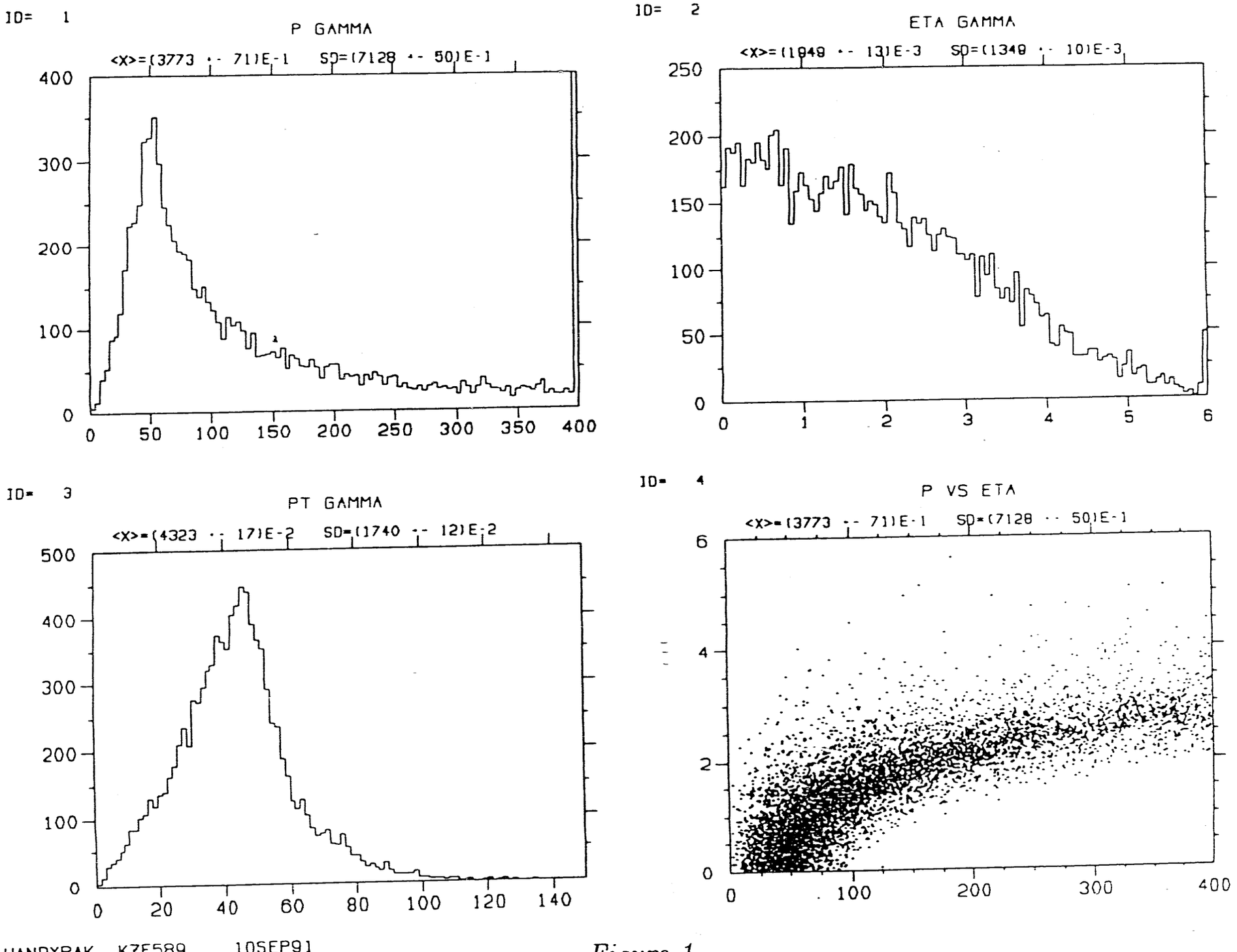
ID= 1
P GAMMA
<X>=(3773 +- 71)E-1 SD=(7128 +- 50)E-1
ID= 2
ETA GAMMA
<X>=(1848 +- 13)E-3 SD=(1348 +- 10)E-3
ID= 3
PT GAMMA
<X>=(4323 +- 17)E-2 SD=(1740 +- 12)E-2
ID= 4
P VS ETA
<X>=(3773 +- 71)E-1 SD=(7128 +- 50)E-1
HANDYPAK KZF589 10SEP91

Figure 1

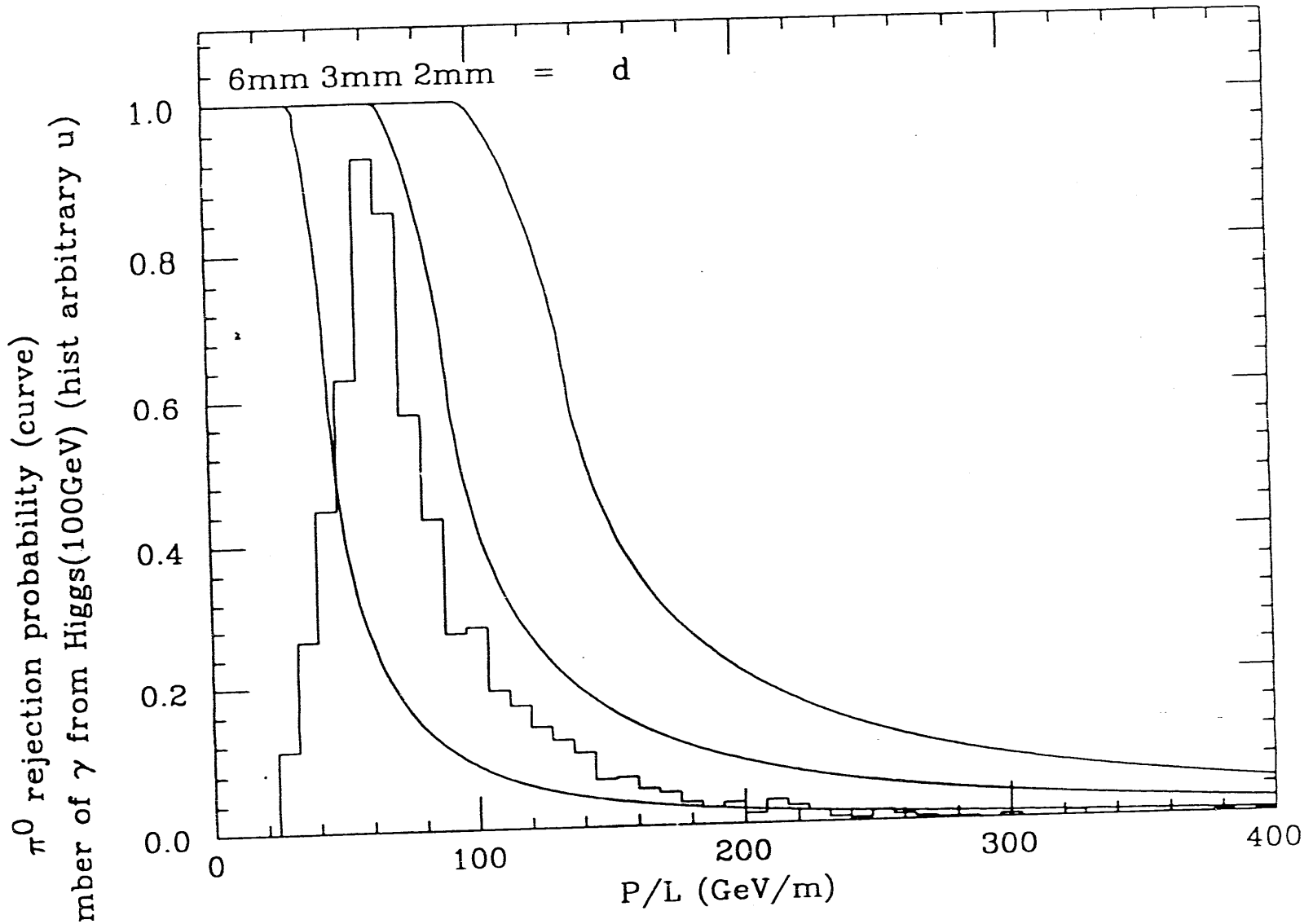
6mm 3mm 2mm = d
π^0 rejection probability (curve)
Number of γ from Higgs(100GeV) (hist arbitrary u)
1.0
0.8
0.6
0.4
0.2
0.0
0
100
200
300
400
P/L (GeV/m)

Figure 2

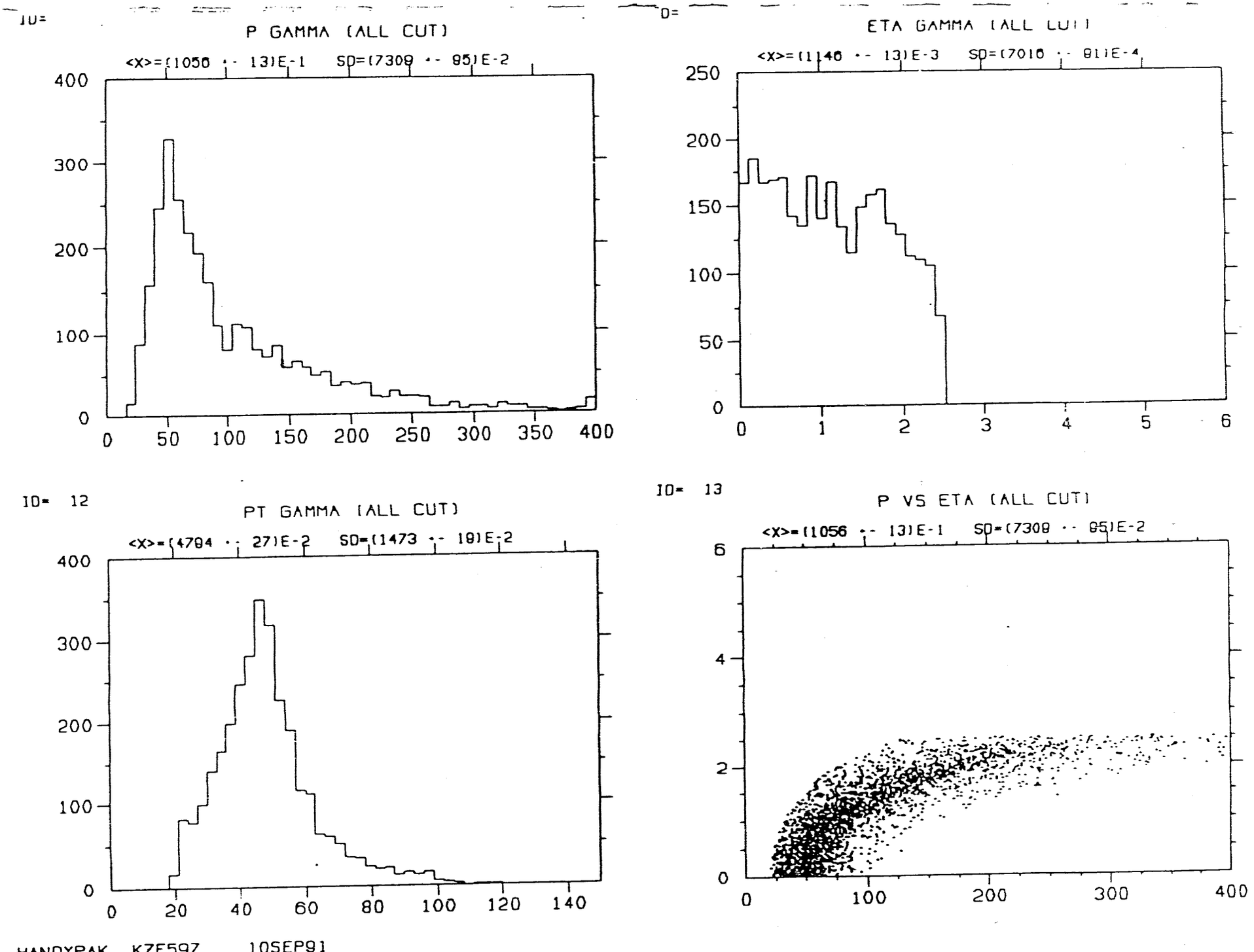
ID=
P GAMMA (ALL CUT)
<X>=(1056 +- 13)E-1 SD=(7309 +- 95)E-2
ID=
ETA GAMMA (ALL CUT)
<X>=(1146 +- 13)E-3 SD=(7016 +- 81)E-4
ID= 12
PT GAMMA (ALL CUT)
<X>=(4784 +- 27)E-2 SD=(1473 +- 18)E-2
ID= 13
P VS ETA (ALL CUT)
<X>=(1056 +- 13)E-1 SD=(7308 +- 95)E-2
HANDYPAK KZF597 10SEP91

Figure 3

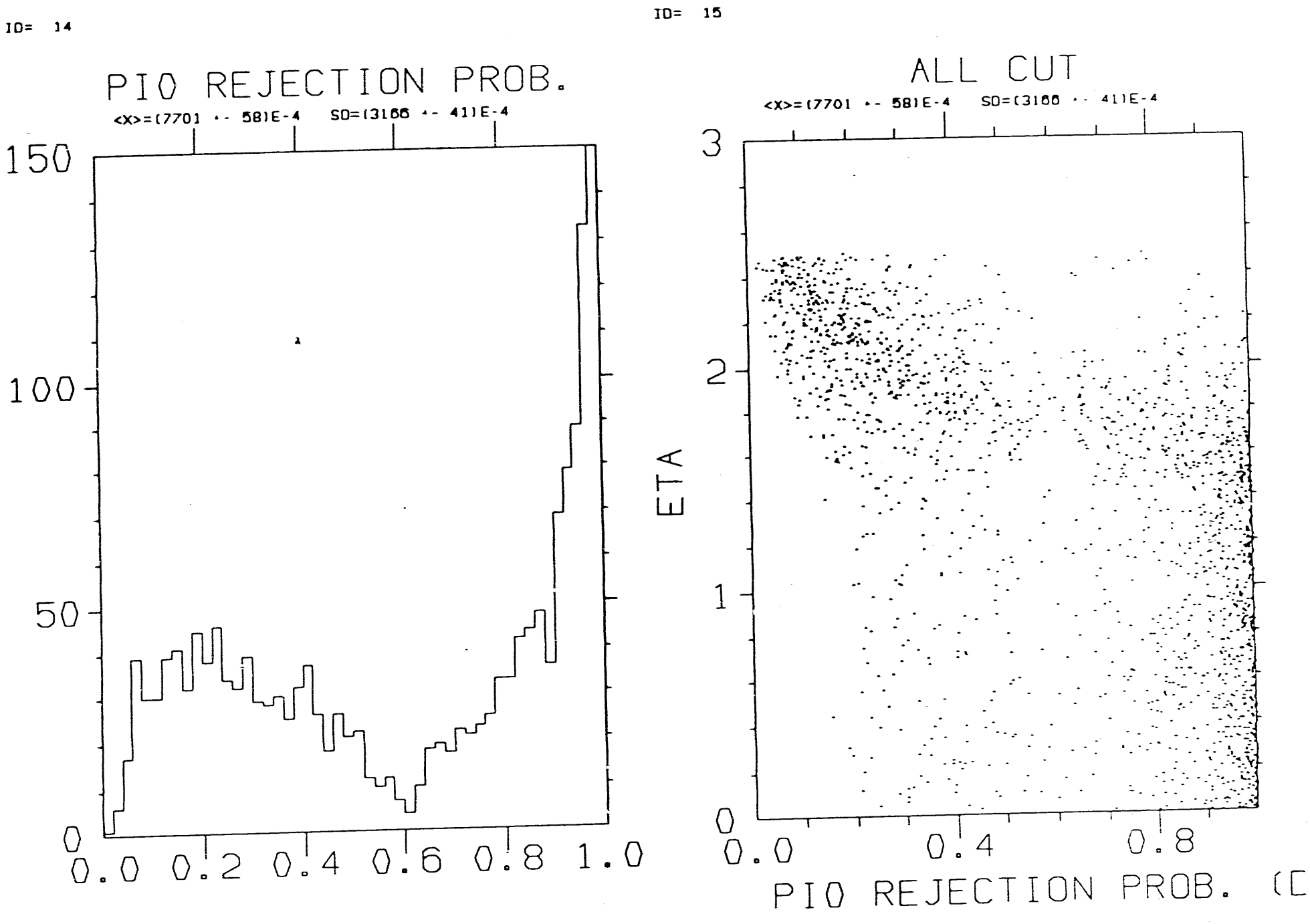
ID= 14
PIO REJECTION PROB.
<X>=(7701 +- 581E-4 SD=(3166 +- 411E-4
150
100
50
0
0.0 0.2 0.4 0.6 0.8 1.0
ID= 15
ALL CUT
<X>=(7701 +- 581E-4 SD=(3166 +- 411E-4
ETA
3
2
1
0
0.0 0.4 0.8
PIO REJECTION PROB. (C
HANDYPAK KZF601 11SEP91

Figure 4

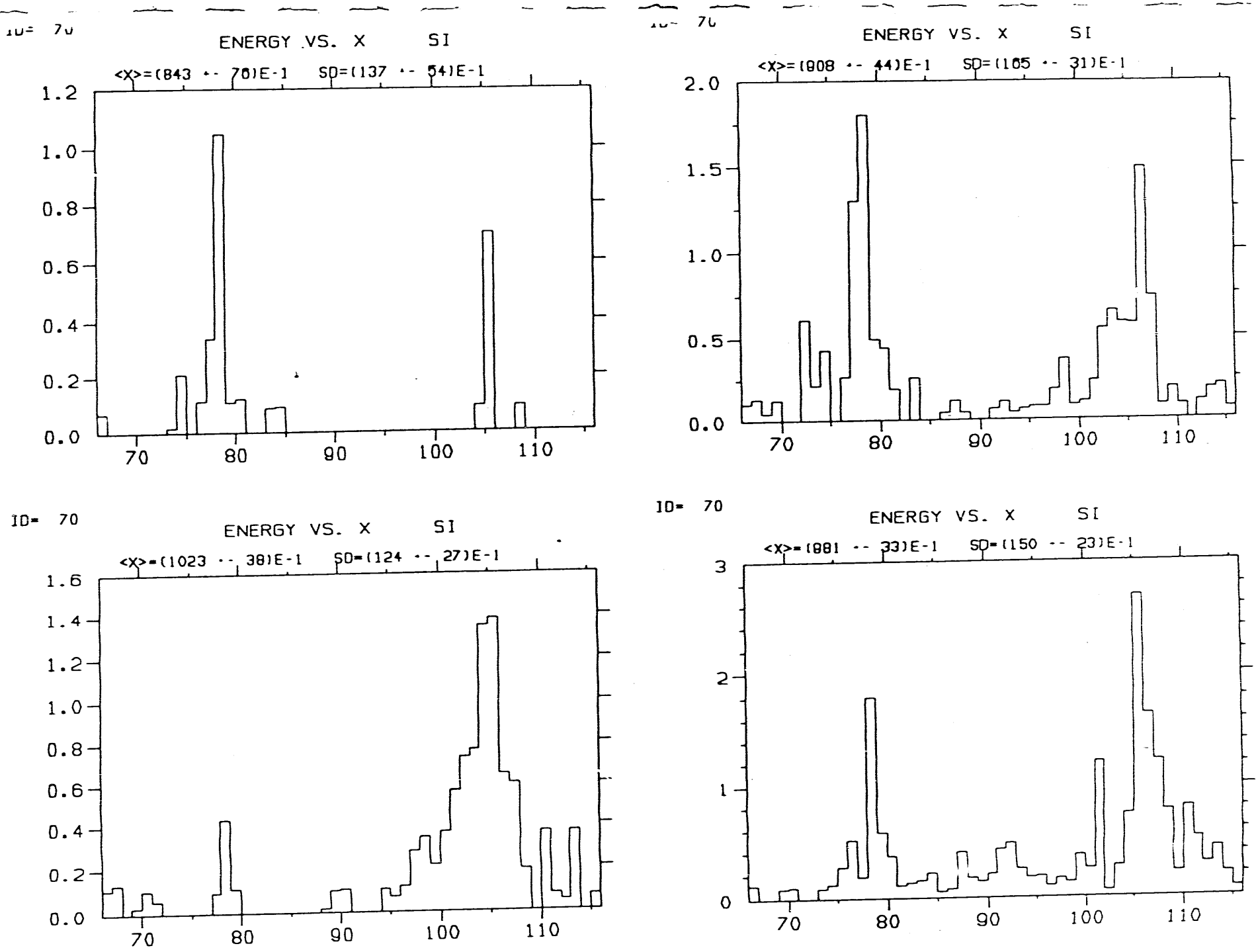
ENERGY VS. X SI
<X>=(843 +- 70)E-1 SD=(137 +- 54)E-1
ENERGY VS. X SI
<X>=(908 +- 44)E-1 SD=(105 +- 31)E-1
ID= 70
ENERGY VS. X SI
<X>=(1023 +- 38)E-1 SD=(124 +- 27)E-1
ID= 70
ENERGY VS. X SI
<X>=(881 +- 33)E-1 SD=(150 +- 23)E-1
HANDYPAK X1A16:42 9SEP91

Figure 5

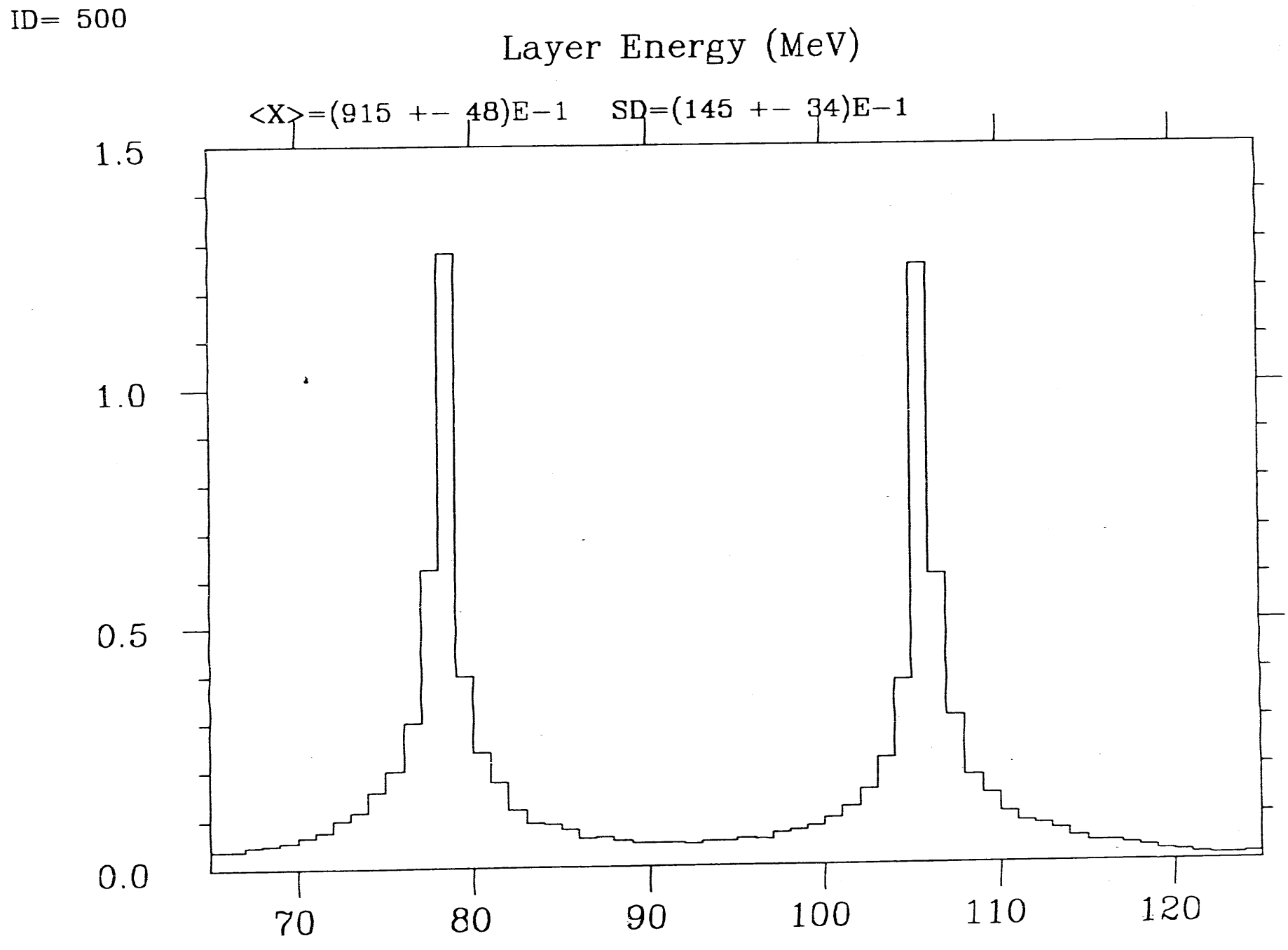
ID= 500
Layer Energy (MeV)
<X>=(915 +- 48)E-1 SD=(145 +- 34)E-1
1.5
1.0
0.5
0.0
70
80
90
100
110
120
HANDYPAK FUR18:17 12NOV91

Figure 6

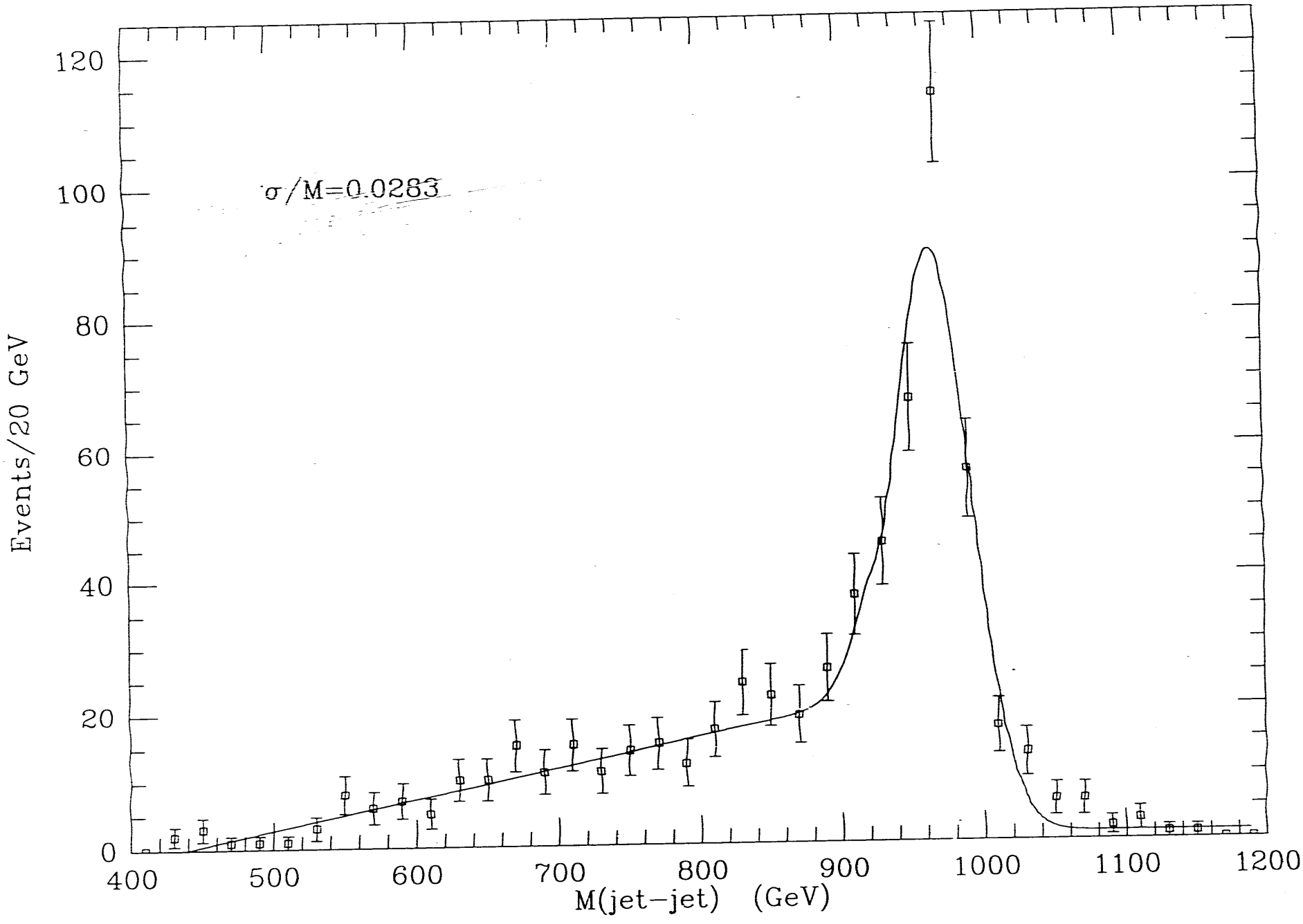
σ/M=0.0283
Events/20 GeV
M(jet−jet) (GeV)
0
20
40
60
80
100
120
400
500
600
700
800
900
1000
1100
1200

Figure 7

5. TAU-CHARM FACTORY

In 1989 the Oregon group became a member of a U.S. tau-charm factory (τcF) collaboration. The focus of the group has evolved during the last two years from that of proposing a U.S. site for a τcF to that of collaborating with European groups toward realization of a site in Europe. Spain has expressed a strong interest in a τcF, and such a proposal is presently under consideration. A brief history and present status follow. The discussion of physics goals and detector design is in the Renewal Proposal.

Discussions of a high luminosity e^+e^- collider operating in the 3–4.2 GeV energy range and a luminosity of $\approx 10^{33}$ cm^{-2}s^{-1}were initiated by Kirkby[1] and Jowett.[2] A workshop was held at SLAC in May, 1989 which helped define the project. An accelerator study of the technical feasibility of a τcF was performed[3] by the U.S. group. In 1990 the site effort shifted to Europe. Spain requested advice from CERN on the technical merits of a τcF. The response[4] was delivered to the Spanish government in November 1990. This report endorsed the technical feasibilty of the τcF and laid out a budget and schedule, calling for completion in 5 years at a cost of 300MSF for accelerator and laboratory, and 90 MSF for the detector. In February, 1991 the Spanish government indicated to CERN that they would provide the funding for the project at a Spanish site. Spain solidified its committment to the τcF by hosting a workshop at the University of Sevilla April 29 - May 2, 1991. Approximately 100 participants took part in physics, detector, and accelerator design discussions. Spain would call on other laboratories, primarily CERN, to provide the necessary technical expertise to build the accelerator. The τcF has been ratified by the CERN scientific policy committee but has not been approved by the CERN Council. The Council has asked that the τcF proponents provide a formal proposal detailing the nature of the collaboration between CERN and Spain.

The U.S. τcF group consists of physicists from SLAC and the Universities of Cincinatti, Illinois, Oregon, Washington, the University of California at Santa Cruz, MIT, Rutgers, and the University of Texas at Dallas.

During the past year, the Oregon group has continued to contribute to design studies for the calorimetry. Examples of this are shown in Figs. 1 and 2. Fig. 1, which was presented at the Sevilla workshop by Ray Frey, shows the distribution of "measured" energy in a $16X_0$ CsI calorimeter for 100 MeV incident photons according to the EGS monte carlo. From such distributions one can determine both the expected energy resolution and the detection efficiency as a function of energy. A paper discussing various CsI performance issues is in preparation. Fig.

2 shows a result on CsI photon position resolution from this work.

References

1. Jasper Kirkby, CERN-EP-87-210 (1987).
2. John Jowett, CERN-LEP-87-56 (1987).
3. B. Barish, *et al.*, SLAC-PUB-5180 (1990).
4. "A Tau-charm Factory Laboratory in Spain...", Y. Baconnier, *et al.*, CERN/AC/90-07 (1990).

FIGURE CAPTIONS

1) EGS simulation of deposited energy in a $16X_0$ CsI as envisioned for a τcF calorimeter. The incident particles are 100 MeV photons.
2) Expected photon position resolution from the showers measured in a τcF CsI calorimeter. The showers are generated by EGS. The positions are based on an energy-weighted mean between towers of the indicated transverse dimensions. The means have been corrected for finite cell-size bias.

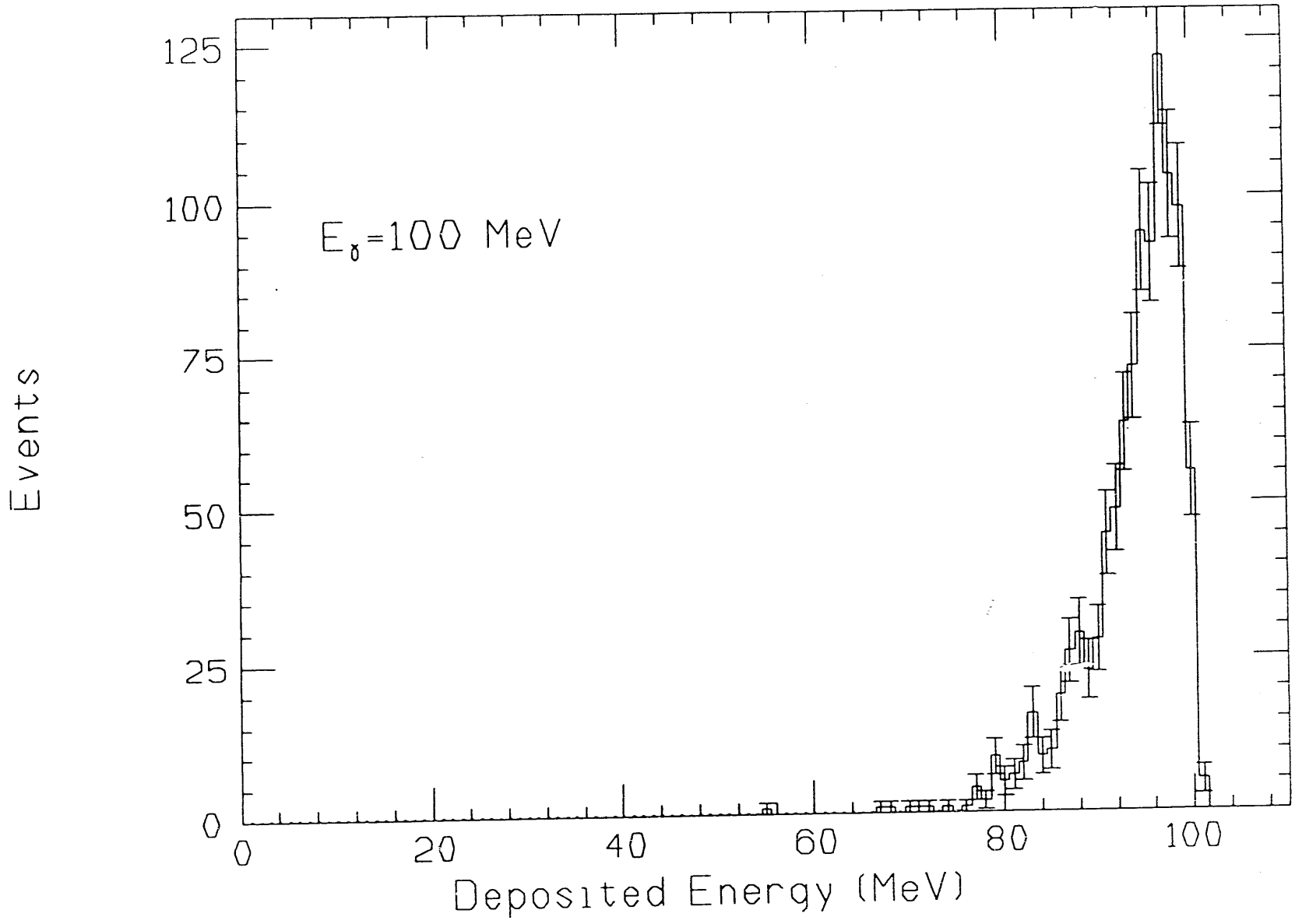
125
100
75
50
25
0
Events
E_γ=100 MeV
0
20
40
60
80
100
Deposited Energy (MeV)

Figure 1

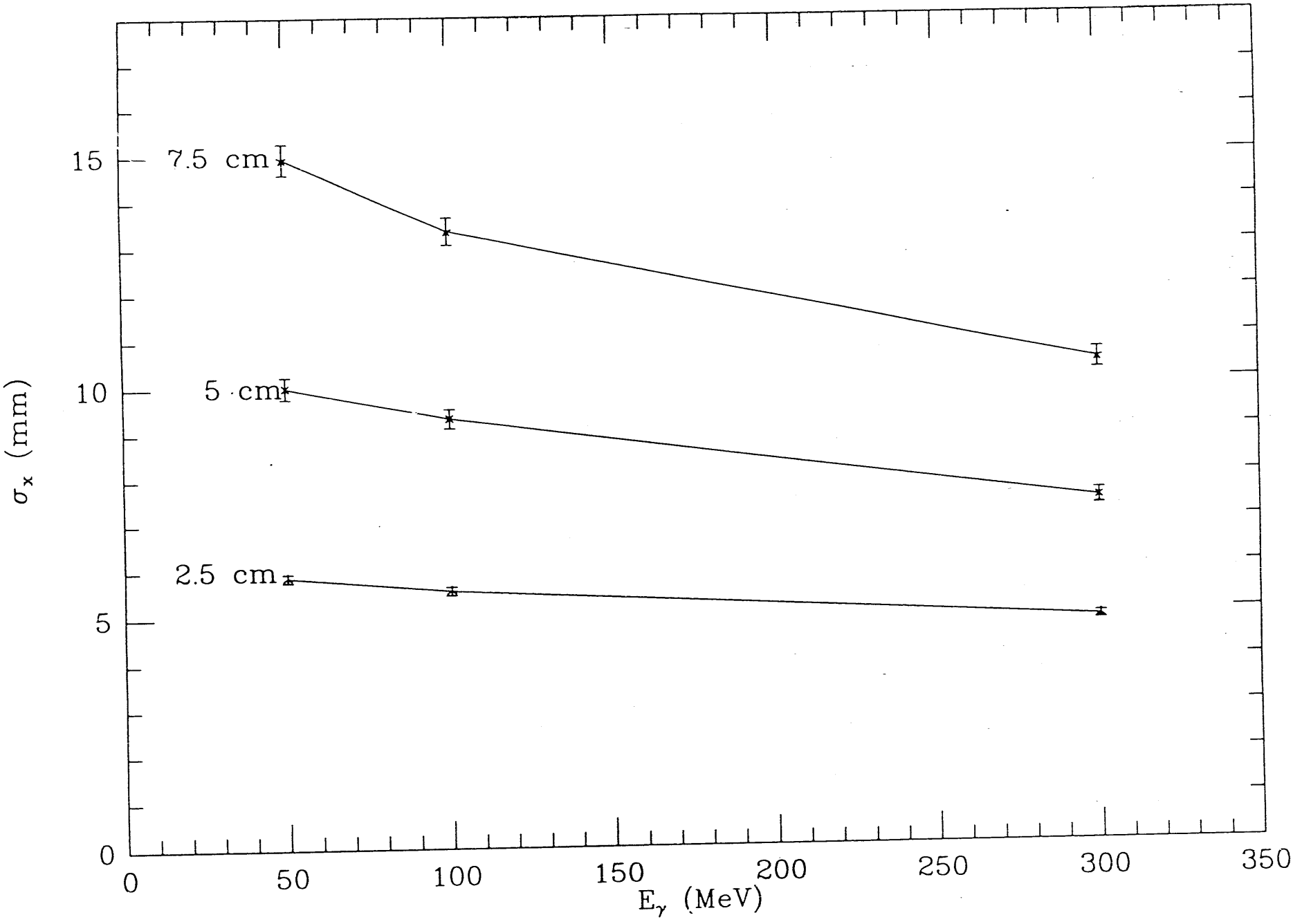
7.5 cm
5 cm
2.5 cm
σ_x (mm)
E_γ (MeV)
0
5
10
15
0
50
100
150
200
250
300
350

Figure 2

6. SECC PRERADIATOR PROTOTYPE AND BEAM TEST

A program is currently underway at Oregon to build a prototype lead/silicon preradiator to be placed in a test beam at Fermilab. The beam should be able to deliver high energy electrons as well as charged pions. This preradiator will be tested in conjunction with the SECC prototype electromagnetic calorimeter. In short, the prototype will consist of at least two 33cm × 33cm planes of silicon detectors and at least one plane of lead of the same cross section. The number and particular arrangement of the silicon and lead layers will be changeable *in situ*. Two types of silicon detectors will be used: 16mm × 16mm pads, and 1mm × 64mm strips. The ORNL preamps being made for SECC will be mounted directly on the detectors using printed circuits which we believe will be similar to that of a complete SSC system. Details are given below.

Beam Test Goals

Apart from the technical knowledge to be gained from the prototype construction, we plan to address the following points from the data which will greatly improve our ability to predict the physics performance of the preradiator:

1. To compare the data with EGS monte carlo for spatial profile and energy deposition of electromagnetic showers.
2. To compare the data with hadron-shower monte carlos (*e.g.* CALOR, GHEISHA) for spatial profile and energy deposition of $\pi^{\pm}$-initiated showers.
3. To determine the ability to resolve nearby electromagnetic showers. (This may require placement of a thin ($\lesssim 1$ L_{rad}) plate in front of the preradiator to provide nearby $e\gamma$ and ee pairs.)
4. To determine the efficiency for electron detection for various radiator thicknesses.
5. To determine the efficiency for MIP detection with fast shaping. (Can a single silicon layer in front of the first radiator plane be an efficient track "stub" detector with fast readout?)
6. To study energy resolution for electromagnetic showers with the preradiator energy added to that of the calorimeter.
7. To determine the position resolution for electromagnetic showers. (This will not be possible if a precise beamline position detector is not available.)
8. To compare strip and pad detectors for the above.

Detector Layout and Mounting

Figure 1 shows the nominal arrangement of radiator and detector planes for the beam test. The detectors (and printed circuits) are affixed to the radiator plates. The prototype structure is being built to allow rearrangement of the planes and addition or removal of radiator.

The radiator is a Pb-Ca-Sn alloy which was used for the SLD liquid argon calorimeter at SLAC. This alloy is significantly more rigid than ordinary Pb plate. The prototype structure could include as many as 6 plates of 6mm thickness and 3 plates of 2mm thickness.

A detector gap is indicated in Figure 2. The gap configuration is essentially the same as that used for the SECC electromagnetic calorimeter (see Section Z). In order to reduce the gap thickness, printed circuits are laid on Kapton. A Kapton layer is affixed to the radiator plate. A positive bias voltage is applied to the silicon detectors via this circuit. The detectors are attached with conductive epoxy. A 3-layer Kapton circuit is then overlaid on the detectors, which routes the input signals, output signals, and power, to the preamplifiers, which are mounted atop the Kapton. The Kapton circuit is attached to the preamps with conductive epoxy inserted into through-plated holes. Figure 3 depicts the placement of the ORNL quad preamps on the pad detectors. Figure 4 shows one of the layers of the Kapton 3-layer circuit which overlays one row of detectors.

The pad detectors were procured as part of the initial purchase of SECC detectors. They have all been received and tested, as described below. As preamplifier prototypes have become available from ORNL, various tests have been performed to study the mechanical structure and electrical properties of the readout configurations shown above. Figure 5 is a pulse from an Am^{241} alpha source on a pad detector with readout via a prototype ORNL CF1X1 preamplifier connected directly to an oscilloscope.

Strip Detectors

Because of the obvious importance of spatial resolution for an SSC preradiator, we have pursued the possibility of narrow rectangular pads, which we can call strips (although "strips" generally connotes a very finely segmented detector for precision tracking). Two layers of crossed strips (X and Y) could then provide excellent position information. The area (and hence capacitance) of each element would be similar to that of a pad array. We have purchased five such detectors from Hamamatsu with elements of size 1mm × 64mm, where each detector consists of 64 such elements. We are readying readout circuits for these strip arrays so that they can be mounted on the prototype and incorporated in the Fermilab beam test.

Preradiator Electronics

Figure 6 indicates schematically what could be the preradiator readout for an SSC system. We believe that it would not be necessary to extend the dynamic range of the readout beyond about 4 bits. This would allow sufficient resolution to discriminate between null/noise, $\pi^{\pm}$-induced showers, and electromagnetic showers. It is not believed that this coarseness would significantly alter the expected resolution for electron and photons, which is based primarily on the electromagnetic calorimeter, but it needs to be studied in greater detail. However, if 4-bit resolution is sufficient, then a significant simplification of the preradiator readout is possible. The preamplifier could have a modest dynamic range. This allows for reduced power consumption and cost per channel. The packaging would perhaps be 8 channels per chip. Presumably an amplifier/shaper stage would then precede the 4-bit flash ADC, followed by a digital pipeline with a depth of approximately 64 beam crossings. A reasonable packaging might include 8 channels each of FADC and digital pipeline per chip.

We have indicated in a very general manner how the preradiator might be included in the trigger. It is not yet clear whether the preradiator information will be an important element in the trigger. The silicon response is intrinsically fast, with charge collection times $\lesssim$10 ns. With the preamplifiers mounted directly on the detectors, this speed could be retained for the trigger if, for example, a slower calorimeter backing the preradiator required a beam-crossing tag for electromagnetic showers. Another possible use for a preradiator trigger would be in the search for any signature requiring a relatively low-energy electron in the trigger. The trigger rate for low-energy electromagnetic clusters would be very high. A fast track "stub" readout – that is, the presence or absence of a MIP track from a coarse silicon pad layer at the front of the preradiator – might be necessary to reduce the trigger rate, which is mostly due to π° production. This needs further study, particularly because of the possibility of running at very high luminosity.

With the goal of maintaining hermetic calorimetry, it is very important to reduce the footprint due to cables carrying the preradiator signals. With the readout sketched above it is hoped that all components would be mounted in close proximity to the detectors. This seems to be feasible. The dissipation of the heat load has to be studied. Then it is assumed that, based on the trigger information, the output could be highly multiplexed to the next level of readout. It is only this reduced set of signals which would be cabled through the detector to the outside. In principle, this is possible since although there may be of order $\sim 5 \times 10^5$ total preradiator channels, the hit multiplicity is low and, furthermore, the number of channels required to be readout to aid with $e/\gamma/\pi$ identification is lower still. How

efficient multiplexing might actually be carried out in practice is under study.

Silicon Procurement

The University of Oregon High Energy Physics Group, in collaboration with the Silicon Electromagnetic Calorimeter Collaboration, and with the support of the Superconducting Supercollider, procured 900 silicon radiation detectors in 1991 for an electromagnetic calorimeter, a silicon preradiator, and radiation damage tests. What follows is a description of the specifications that were given to the vendor.

SILICON DETECTOR ARRAY SPECIFICATIONS

Three unique array types are required for the project. Figures 7-9 specify the dimensions and tolerances for the three. These figures specify the active area dimensions. All detectors have an active area of 64 mm by 64 mm and are subdivided into either 4 (2 by 2), 16 (4 by 4), or 36 (6 by 6) cells. They are referred to as designs O4, O16, O36. The quantity of arrays needed for each type are:

type	EM cal	prerad	rad damage	spares	total
O16	396	25		49	470
O36	24	25		11	60
O4	280		60	30	370
Total					900

All specifications below are defined at room temperature (25 C).

The front metalization shall be one-half to two and one-half microns thick aluminum. The detectors shall be n-type silicon with the positive implant (or dopant) on the front (divided) side. The back metalization shall be one-half to one micron thick aluminum and shall completely and continuously cover the back surface, thus forming a common ground for all segments within an array. The silicon shall have a nominal thickness of 300 microns. The thickness of all devices shall be within ± 4% of that value. The cells

must fully deplete at less than 100 VDC. Full depletion is defined here as the point at which the cell's capacitance is within 2% of the asymptotic value of the cell's minimum capacitance. The breakdown voltage is defined as that voltage which when applied to a cell results in a current of 10 microAmps or greater. Based on this definition, all detectors shall have a breakdown voltage of greater than one and one-half times the full depletion voltage. One operating voltage must be specified for all detectors such that they are all fully depleted and their leakage currents meet the following tolerances, at that voltage. Ninety five percent (95%) of the cells must have leakage currents of less than 100 nanoAmps. Five percent (5%) of the cells may exceed 100 nanoAmps but they must not exceed 500 nanoAmps. One hundred percent (100%) of the cells must be operational. No array can have more than two cells exceeding the 100 nanoAmp limit. Each array will be tested and graded by U of O. Grading will be as follows. Grade 1 will be assigned if all cells of an array meet or exceed the 100 nanoAmp specification; Grade 2, if one cell fails it, but it is less than 500 nanoAmps; Grade 3, if two cells fail it, but each is less than 500 nanoAmps; Grade 4, if the array is not acceptable. The results of the grading can be made available to the manufacturer within thirty (30) days of receipt of the devices by the University of Oregon. For any array rejected, the U of O group will supply the manufacturer with lab data indicating our measurements of cell leakage currents, capacitances, etc.

The intercell resistivity must exceed 10 Megohms for all cells. The crosstalk between any two cells of an array must be less than 1.0%. We measure this type of crosstalk by comparing the response of any cell in the array to that of any other cell in the array which has a Americium-241 alpha source (5.5 MeV) radiating towards it's center.

Each detector array shall be uniquely identified with a serial number that is attached to the detector. The numbering scheme will be agreed upon by the manufacturer and U of O.

The manufacturer shall provide U of O with a cell by cell QC-type production data sheet for each array. It shall include as a minimum, the following information: array serial number and type, depletion voltage of each cell, the leakage currents for each cell at three or more voltages (with a least one measurement below and one at twice the depletion voltage), and the nominal thickness of the

array.

DRAWINGS

The attached figures 7-9 specify the dimensions of the detectors. The surfaces of the diodes that are required to be left uncovered by passivation are indicated with the broken lines. These *pads* will be used for electrical contact. As is shown, all detectors have an active area of 64 mm by 64 mm and are subdivided into either 4 (2 by 2), 16 (4 by 4), or 36 (6 by 6) cells. The edge will be cut as closely to the active area as possible, but no more than 500 microns.

RELIABILITY

In an effort to calculate the total calorimeter reliability, U of O requests that the manufacturer provide any immediately available reliability data on their detectors. Data of interest would include: expected cell leakage current drift as a function of time; cell degradation due to radiation/particle bombardment; and effects and limits of mechanical stress.

Full delivery of this order was achieved by late March and testing was completed at the University of Oregon by April 10, 1991. The test procedure called for measuring the capacitance-voltage and leakage current-voltage characteristic of every cell (11,160 in total). Figures 10-12 show the distributions of the measured leakage currents of the three types of cells.

The following table summarizes the delivery of the detectors and the testing schedule.

Date	O4-			O16-			O36		
	deliv.	tested	acceptd	deliv	tested	acceptd	deliv	tested	acceptd
2/28	187	25	25	274	162	161	39	4	4
3/06	281			377			60		
3/08	370	25	25	419	244	243	60	22	22
3/15	370	25	25	470	346	345	60	22	22
3/22	370	106	106	470	448	447	60	22	22
3/29	370	294	294	470	470	469	60	22	22
4/10	370	370	370	470	470	469	60	60	60

Most of these detectors were delivered to the SECC collaborators for their use. The detectors were delivered from Oregon as follows:

February 2, 1991:

shipped to University of Tennessee:

4 4-cell devices

4 16-cell devices

4 36-cell devices

April 19, 1991

shipped to University of Tennessee:

43 4-cell devices

230 16-cell devices

April 26, 1991

shipped to University of Tennessee:

253 4-cell devices

205 16-cell devices

26 36-cell devices

May 31, 1991

shipped to Carnegie Mellon:

60 4-cell devices

A total of 829 detectors were distributed to the SECC Collaboration, having been carefully tested and accepted. Only one detector was rejected. It arrived in Eugene broken and was returned to the vendor. Seventy detectors were kept at the University of Oregon for use in the preradiator work.

FIGURE CAPTIONS

1) Nominal arrangement of radiator and detector planes for the preradiator prototype beam test.
2) Preradiator prototype detector gap.
3) Placement of the ORNL quad preamps on the pad detectors.
4) One of the layers of the Kapton 3-layer circuit which overlays one row of detectors.
5) Single pulse from an Am^{241} alpha source on a pad detector.
6) Possible preradiator readout scheme for an SSC system.
7) Drawing of a 64 mm by 64 mm detector, in this case subdivided into 6×6 separate cells.
8) Drawing of a 64 mm by 64 mm detector, in this case subdivided into 4×4 separate cells.
9) Drawing of a 64 mm by 64 mm detector, in this case subdivided into 2×2 separate cells.
10) Distribution of leakage currents for SECC detectors, in this case for the 6×6 detectors.
11) Same as Fig. 10, but for the 4×4 detectors.
12) Same as Fig. 10, but for the 2×2 detectors.

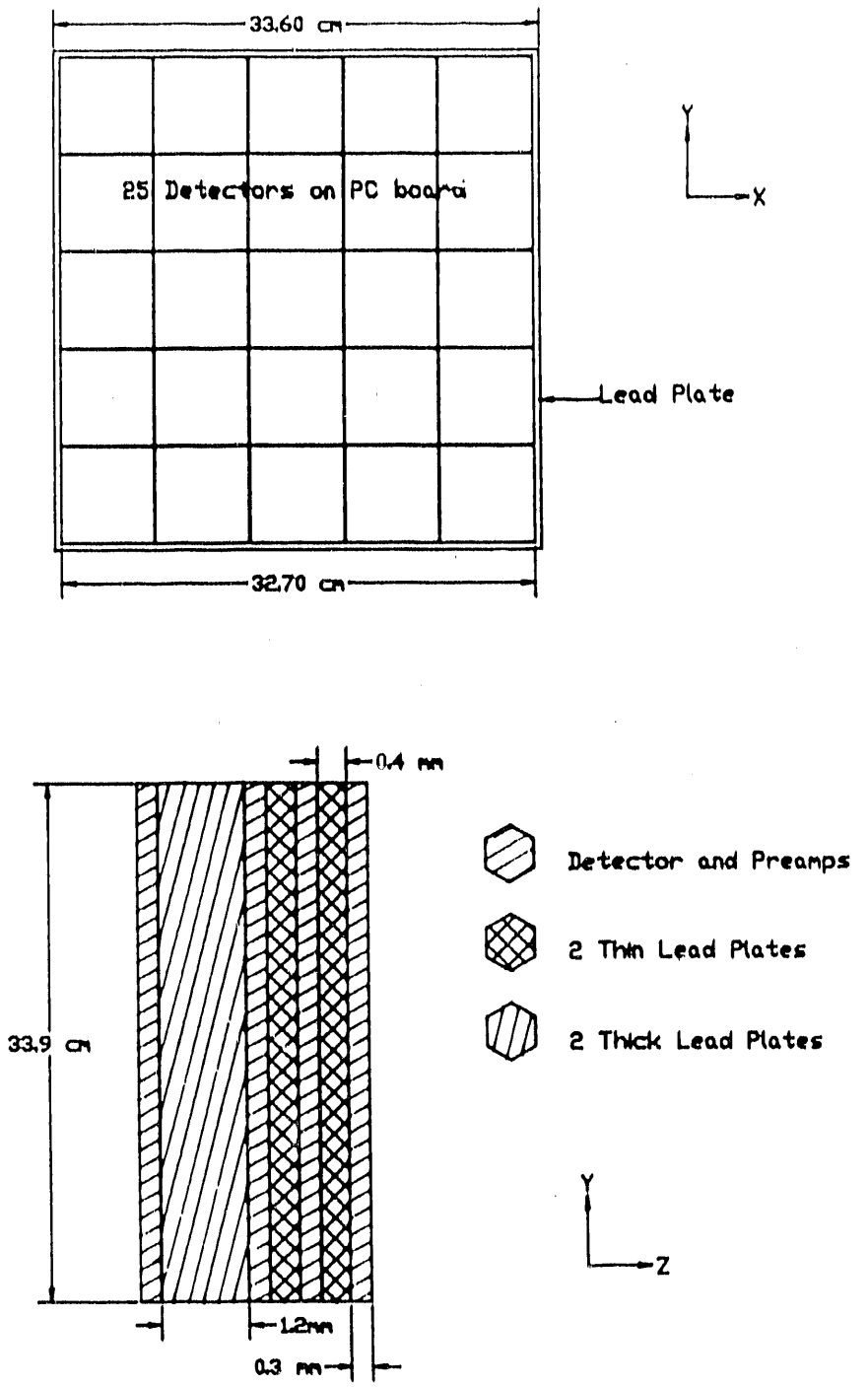
33.60 cm
25 Detectors on PC board
Y
X
Lead Plate
32.70 cm
0.4 mm
33.9 cm
Detector and Preamps
2 Thin Lead Plates
2 Thick Lead Plates
Y
Z
1.2mm
0.3 mm

Figure 1

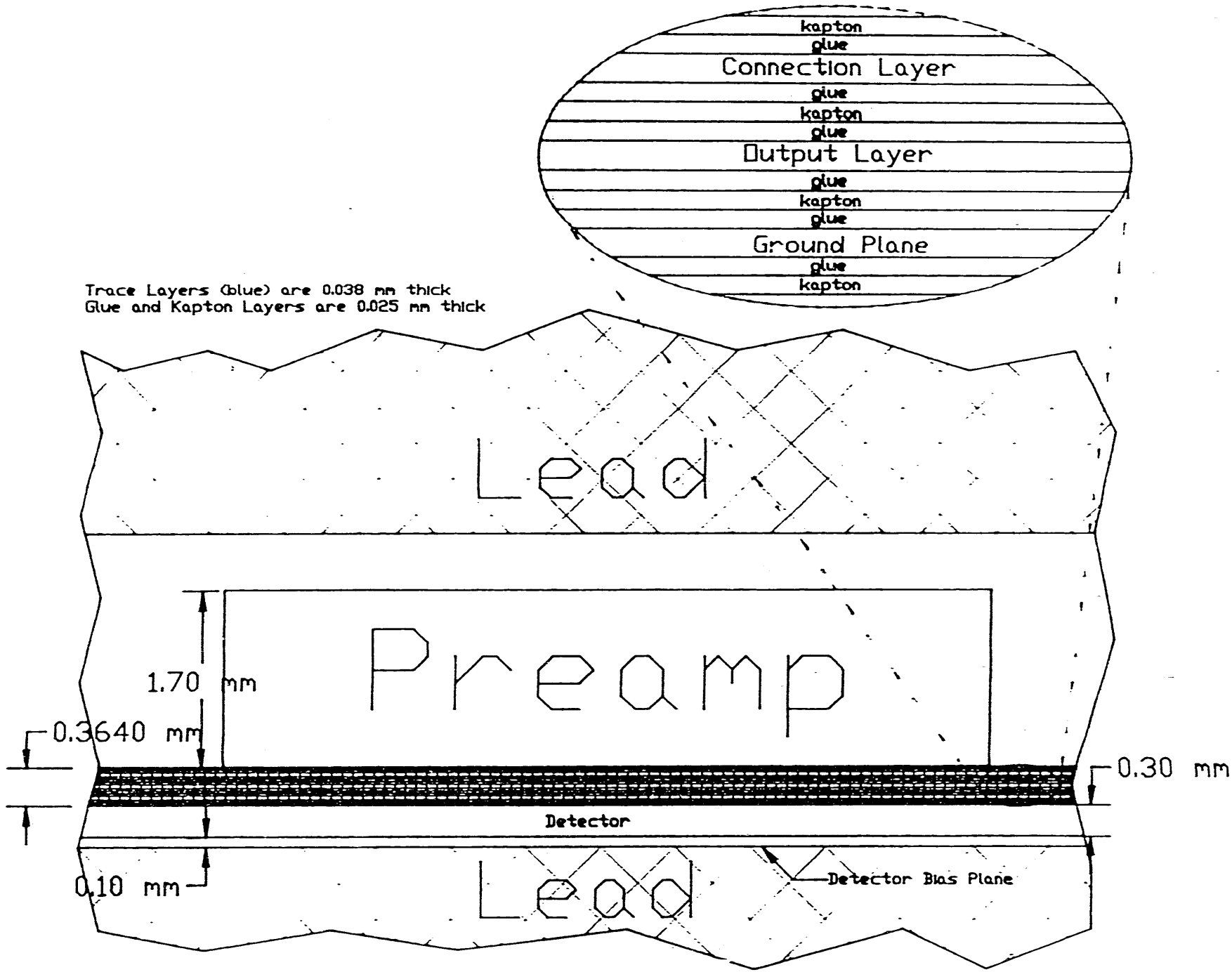
kapton
glue
Connection Layer
glue
kapton
glue
Output Layer
glue
kapton
glue
Ground Plane
glue
kapton
Trace Layers (blue) are 0.038 mm thick
Glue and Kapton Layers are 0.025 mm thick
Lead
Preamp
1.70 mm
0.3640 mm
0.30 mm
Detector
0.10 mm
Lead
Detector Bias Plane

Figure 2

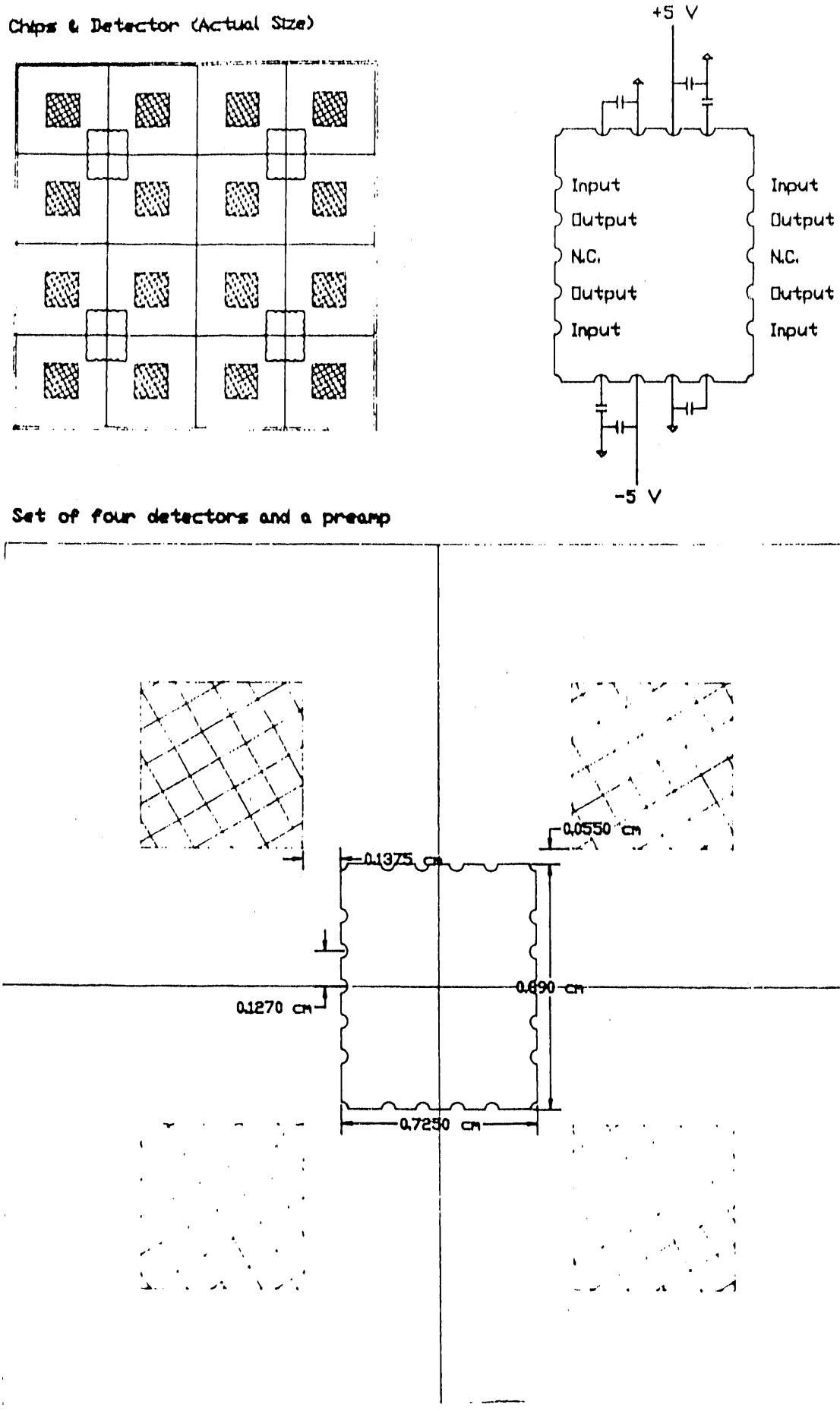
Chips & Detector (Actual Size)
+5 V
Input
Output
N.C.
Output
Input
Input
Output
N.C.
Output
Input
-5 V
Set of four detectors and a preamp
0.0550 cm
0.1375 cm
0.690 cm
0.1270 cm
0.7250 cm

Figure 3

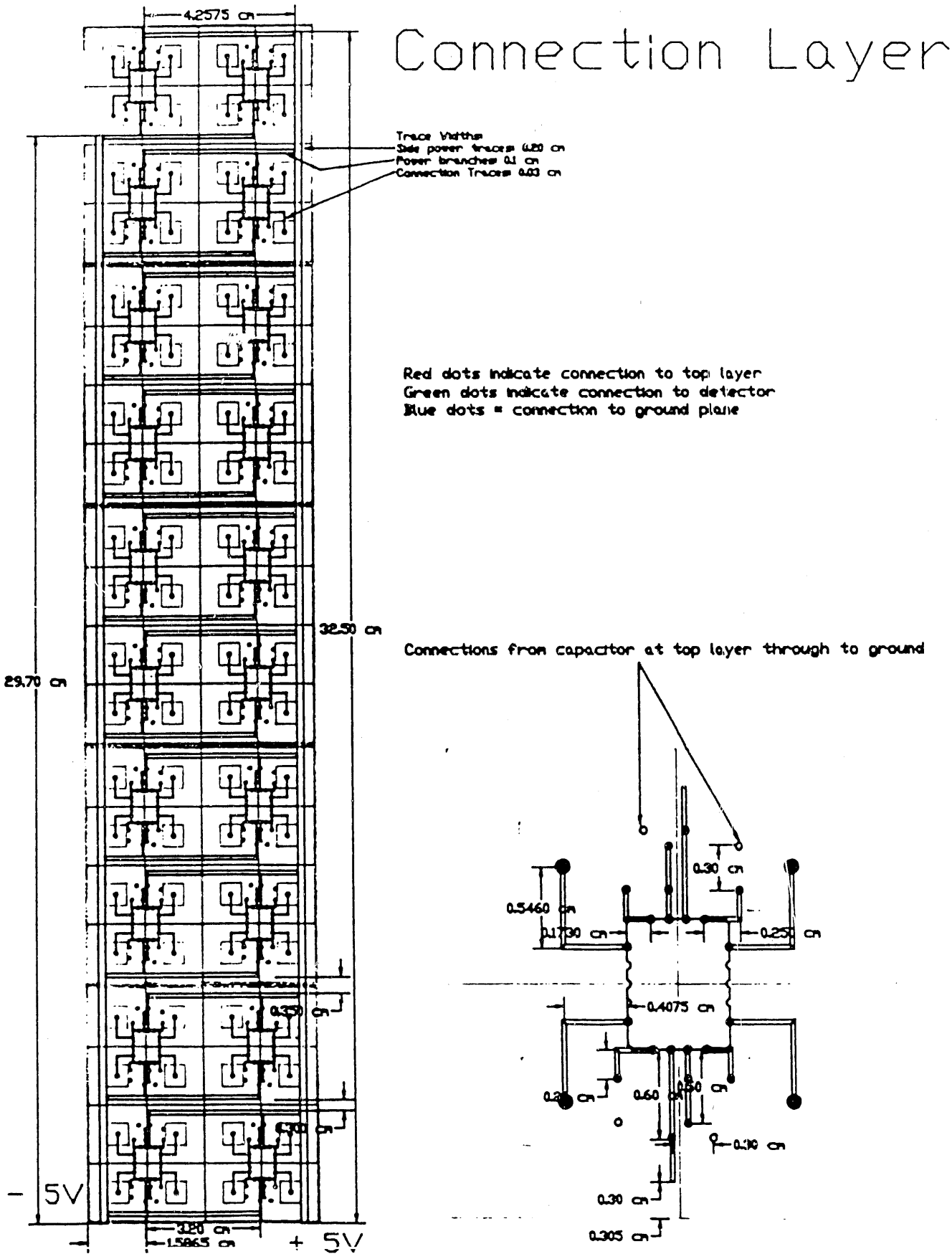
Connection Layer
4.2575 cm
Trace Widths
Side power traces 0.20 cm
Power branches 0.1 cm
Connection Traces 0.03 cm
Red dots indicate connection to top layer
Green dots indicate connection to detector
Blue dots = connection to ground plane
32.50 cm
29.70 cm
Connections from capacitor at top layer through to ground
0.30 cm
0.5460 cm
0.1730 cm
0.25 cm
0.4075 cm
0.60 cm
0.30 cm
0.30 cm
0.305 cm
- 5V
+ 5V
3.20 cm
1.5865 cm

Figure 4

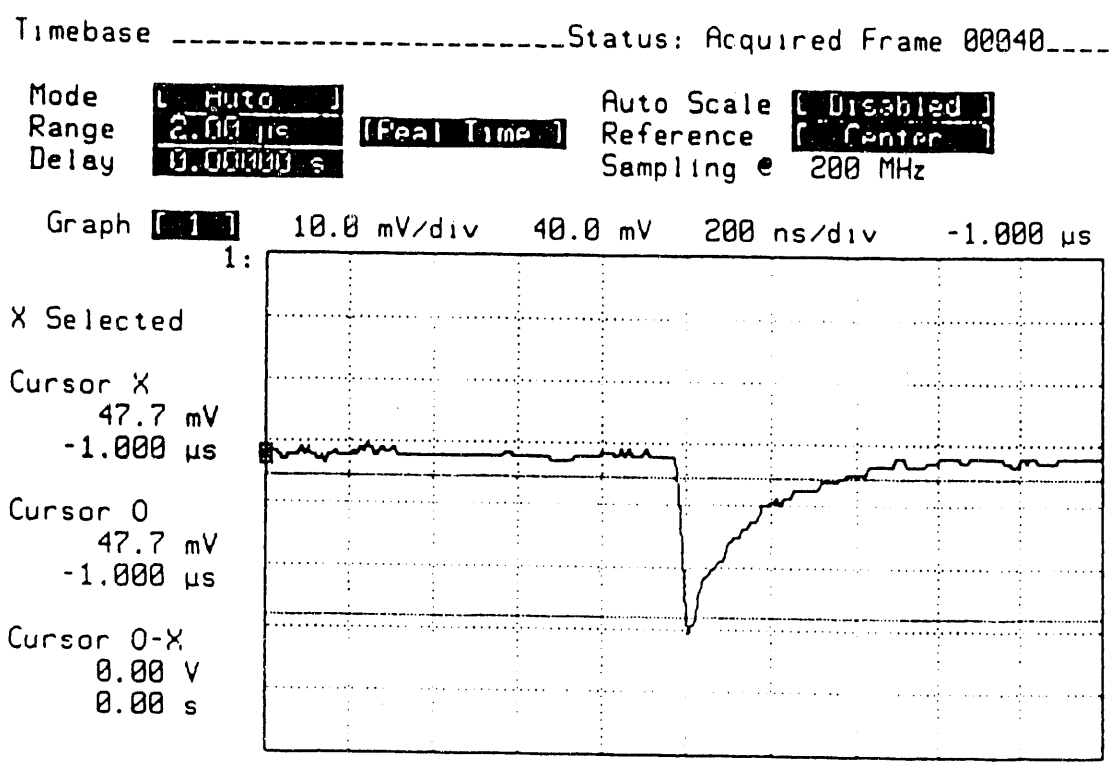
Timebase
Status: Acquired Frame 00040
Mode
Range
Delay
[Auto]
2.00 µs
0.000000 s
[Real Time]
Auto Scale
Reference
Sampling @
[Disabled]
[Center]
200 MHz
Graph [1]
10.0 mV/div
40.0 mV
200 ns/div
-1.000 µs
1:
X Selected
Cursor X
47.7 mV
-1.000 µs
Cursor O
47.7 mV
-1.000 µs
Cursor O-X
0.00 V
0.00 s

Figure 5

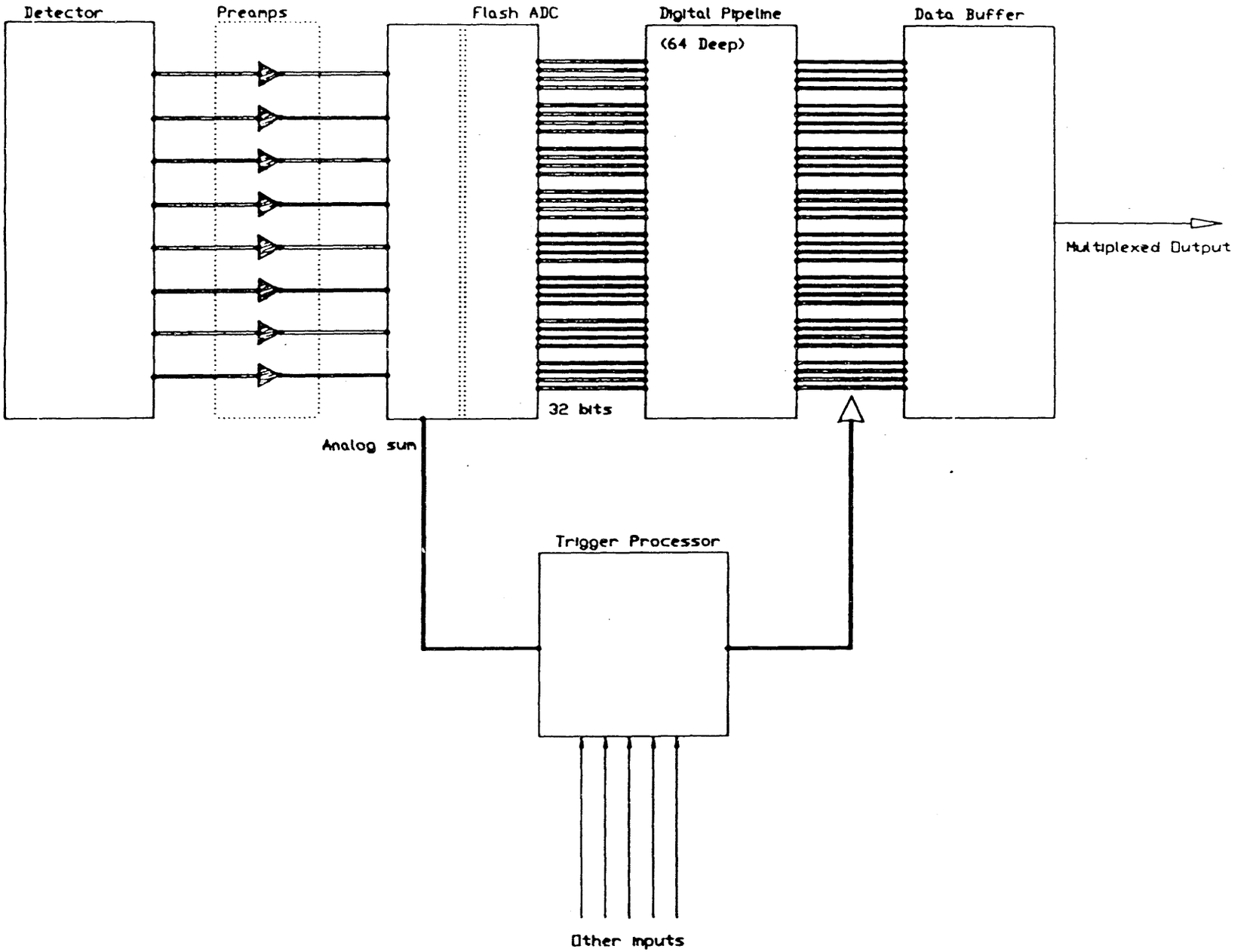
Detector
Preamps
Flash ADC
Digital Pipeline
(64 Deep)
Data Buffer
Multiplexed Output
32 bits
Analog sum
Trigger Processor
Other Inputs

Figure 6

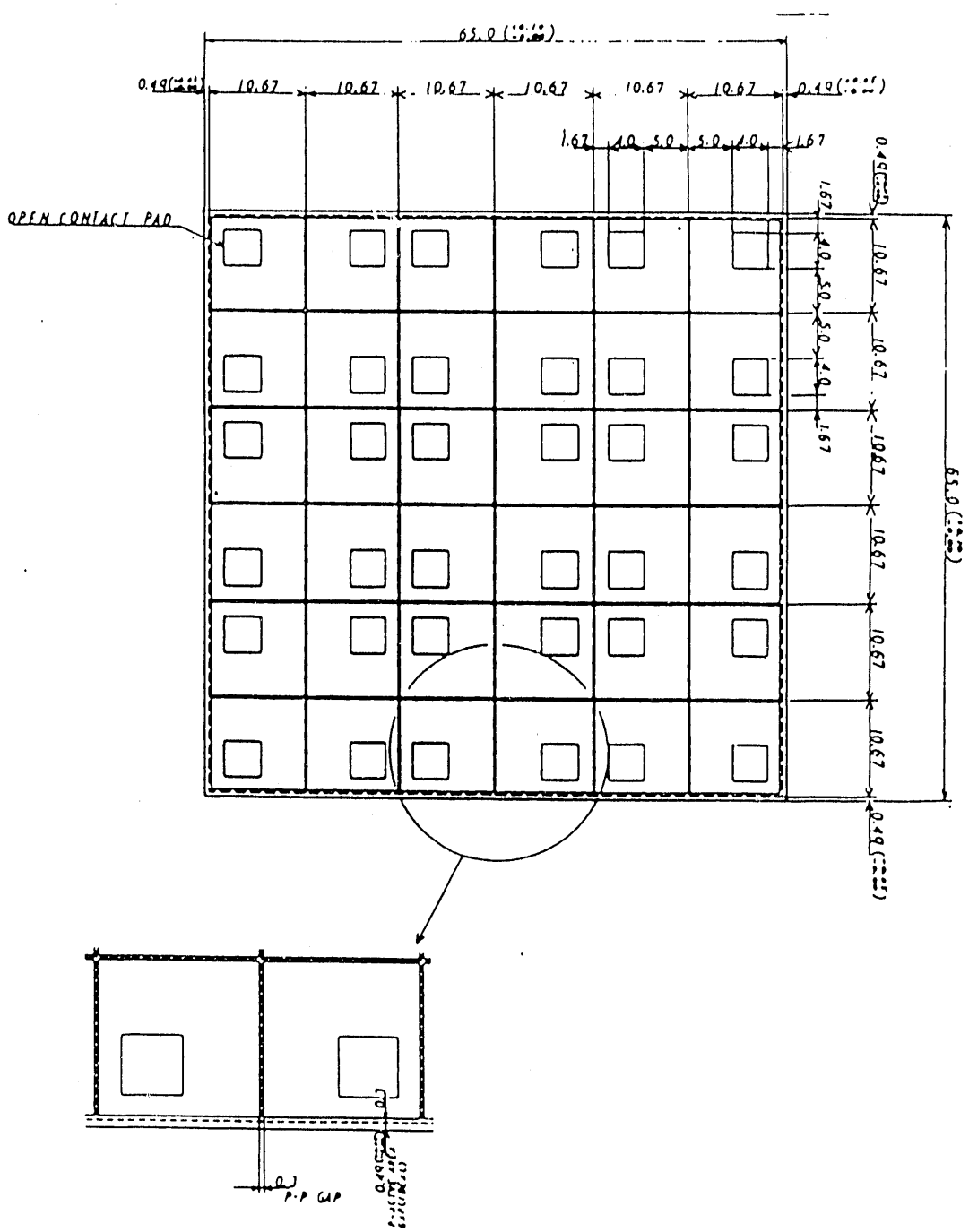

ITEM	REVISIONS	DATE	APPROVED	UNIT	mm	SCALE	2.5/1	NAME	64X64 DETECTOR(036)	DATE	'90.10.24
				APPROVED: H. Aoyi				DWG NO.	350379	REV	UNIV. OF OREGON
				CHECKED: H. Aoyi							
				DRAWN: H. Ishikawa					HAMAMATSU PHOTONICS K.K.		
				DESIGNED: H. Ishikawa					1126-1 ICHINO HAMAMATSU JAPAN		

Figure 7

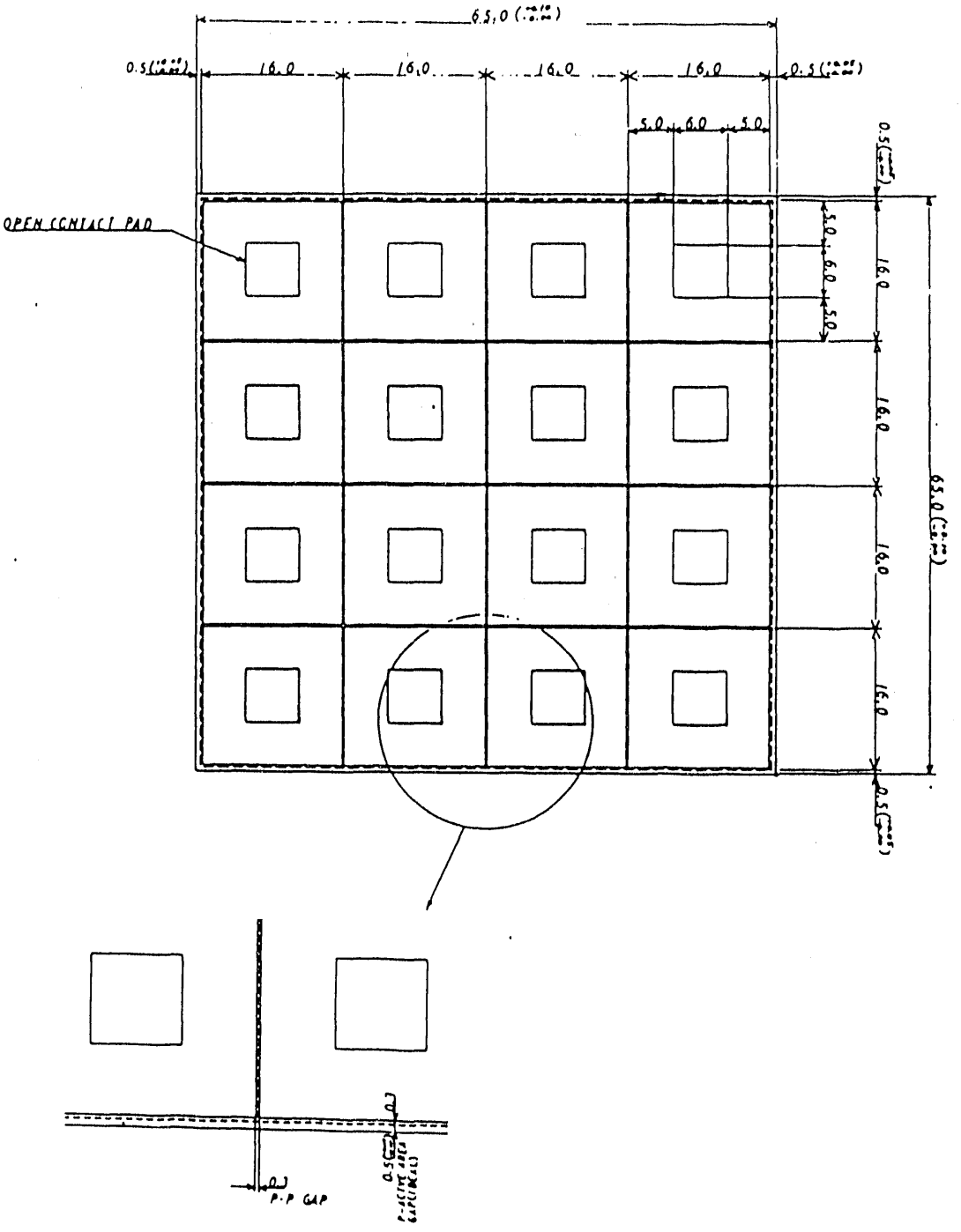

				UNIT	mm	SCALE	2.5/1	NAME	64X64 DETECTOR(016)	DATE	'90.10.24
				APPROVED	H.A-V			DWG. NO.	350378	REF	UNV. OF OREGON
				CHECKED	H.A-V						
				DRAWN	Y.Ishikawa						
ITEM	REVISIONS	DATE	APPROVED	DESIGNED	Y.Ishikawa				HAMAMATSU PHOTONICS K.K.		

Figure 8

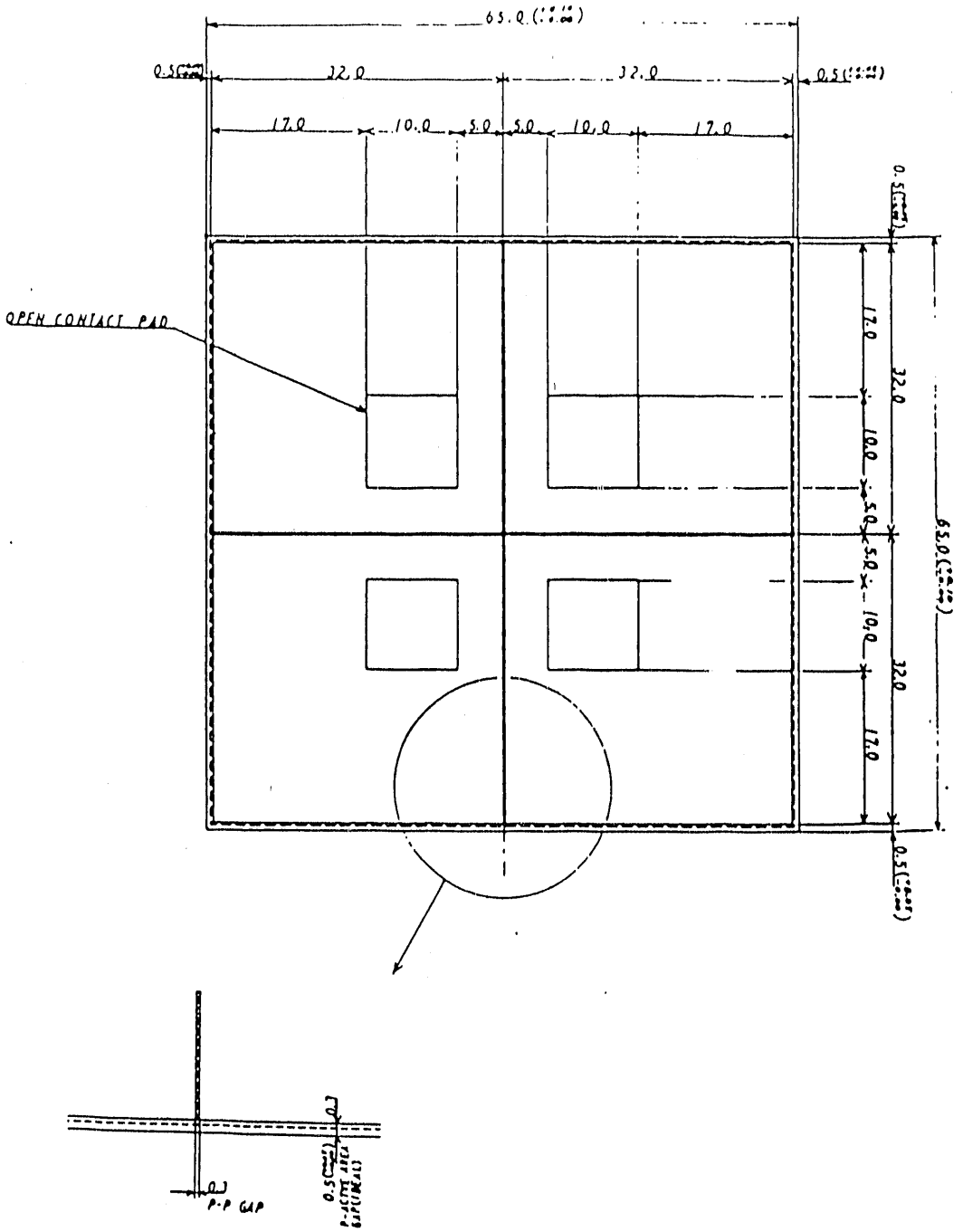

				UNIT	mm	SCALE	2.5/1	NAME	64X64 DETECTOR(04)	DATE	'90.10.24
				APPROVED: H. Akiba				DWG NO.	350377	REF	UNV. OF OREGON
				CHECKED: H. Akiba				HAMAMATSU PHOTONICS K.K.			
				DRAWN: Y. Ishikawa				1126-1 ICHINO HAMAMATSU JAPAN			
ITEM	REVISIONS	DATE	APPROVED	DESIGNED: Y. Ishikawa							

Figure 9

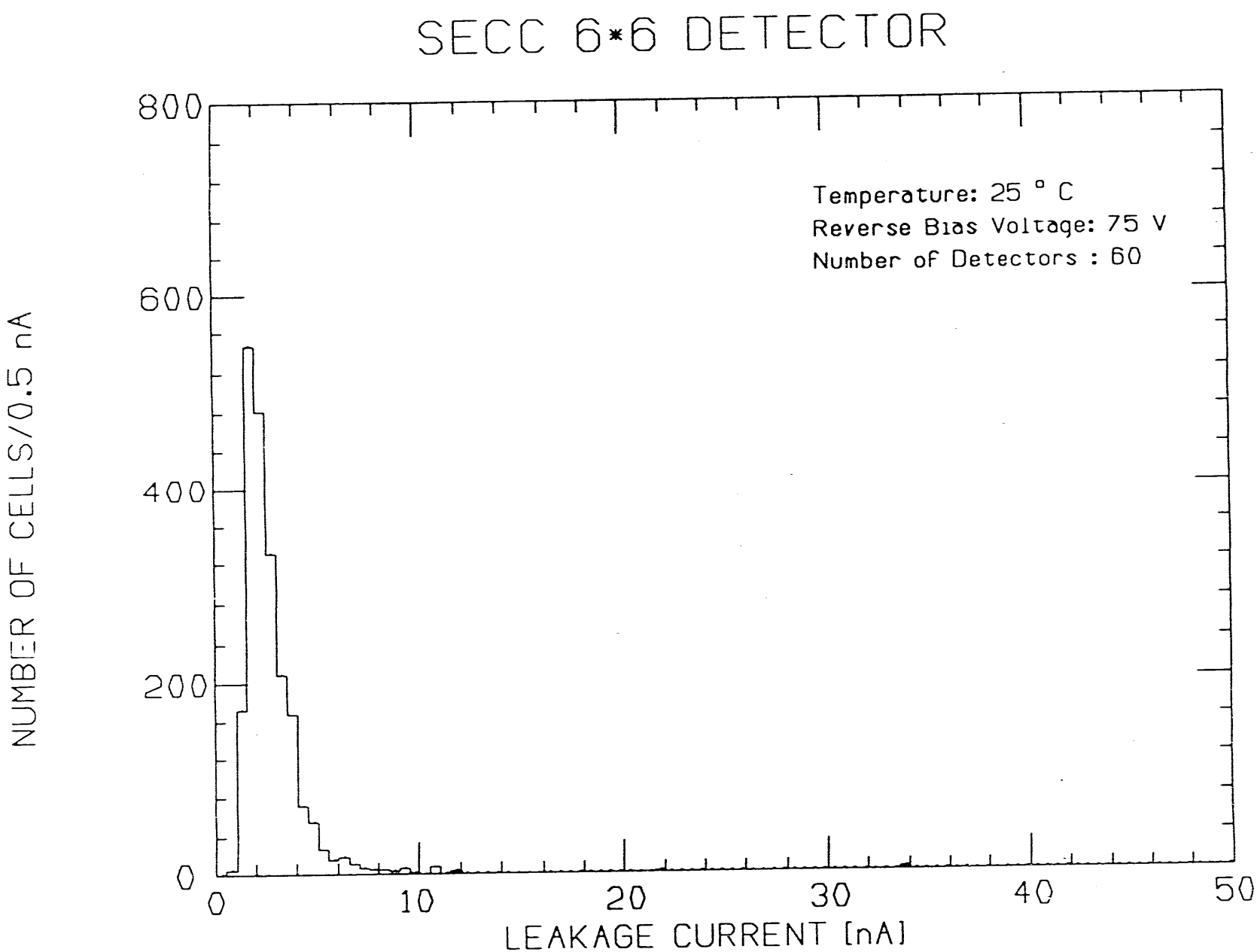
SECC 6*6 DETECTOR
Temperature: 25 ° C
Reverse Bias Voltage: 75 V
Number of Detectors : 60
NUMBER OF CELLS/0.5 nA
LEAKAGE CURRENT [nA]
0
200
400
600
800
0
10
20
30
40
50

Figure 10

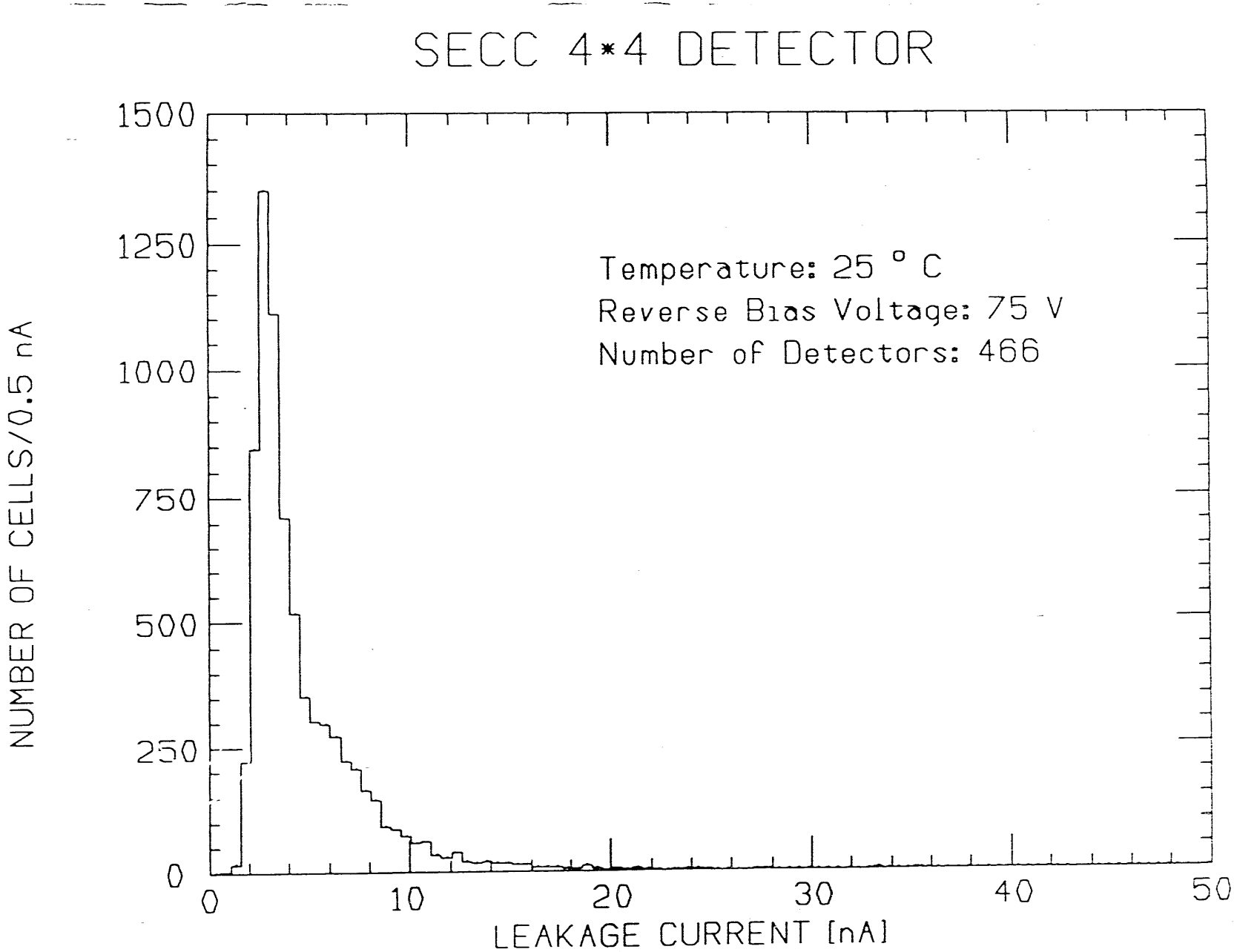
SECC 4*4 DETECTOR
Temperature: 25 ° C
Reverse Bias Voltage: 75 V
Number of Detectors: 466
NUMBER OF CELLS/0.5 nA
LEAKAGE CURRENT [nA]
0
250
500
750
1000
1250
1500
0
10
20
30
40
50

Figure 11

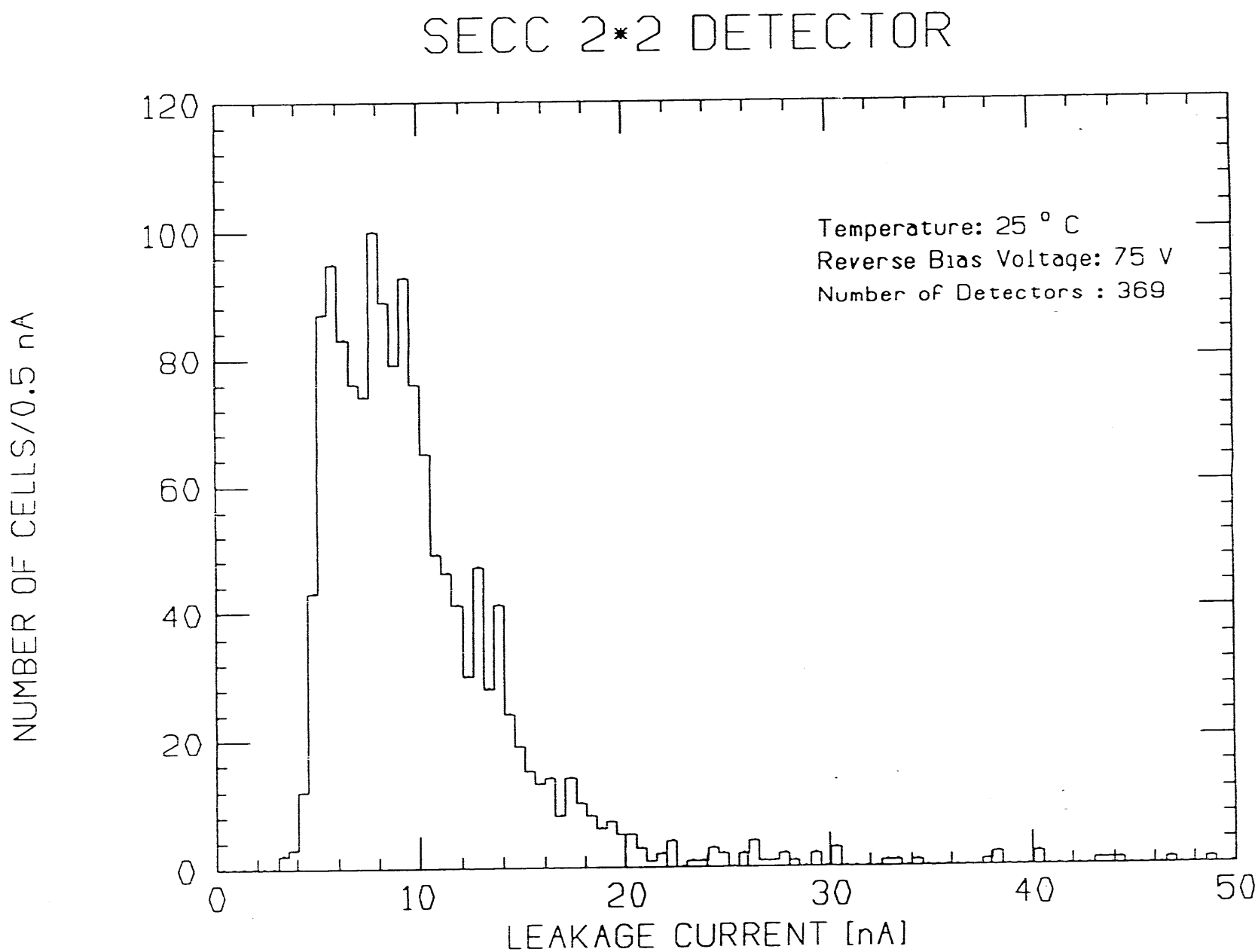
SECC 2*2 DETECTOR
Temperature: 25 ° C
Reverse Bias Voltage: 75 V
Number of Detectors : 369
NUMBER OF CELLS/0.5 nA
LEAKAGE CURRENT [nA]
0
20
40
60
80
100
120
0
10
20
30
40
50

Figure 12

7. List of publications and papers for last year

See the vita in the proposal.

8. Foreign trips for Nov 1, 1990-Sep 30, 1991

Ray Frey - Tau-charm Workshop, Sevilla, Spain,
April 29 - May 2, 1991.

Jim Brau - Lepton-Photon Symposium, Geneva, Switzerland,
July 24 - August 2, 1991.
(supported by the Texas National Research Laboratory Commission)

9. Personnel

The personnel working on this grant during the past year have been:

Jim Brau	Professor
Ray Frey	Assistant Professor
David Strom	Assistant Professor (since Sep 91)
Koichiro Furuno	Postdoctoral Research Associate
Cary Zeitlin	Postdoctoral Research Associate (located at SLAC)
Charles Beauvais	graduate student
Hyun Hwang	graduate student
Matt Langston	graduate student
Hwanbae Park	graduate student (located at SLAC)
Kevin Pitts	graduate student (located at SLAC)
Xiao Qing Yang	graduate student
Jing Chen Zhou	graduate student
Russsell Evans	undergraduate student
Steve Lundgren	undergraduate student
Dave Mason	undergraduate student
Phil Pearson	undergraduate student

END

DATE FILMED

7/2/92